21)
HUDSON LABORATORIES of Columbia University
145 Palisade Street, Dobbs Ferry, N.Y. 10522

Technical Report No. 158

SUMMARY REPORT, ATMOSPHERIC PROPAGATION BACKGROUND STUDIES UP TO SEPTEMBER 1, 1968

by
Ivan Tolstoy
T. Herron
E. Bendor
D. W. Kraft

September 1968

Contract Nonr-266(84)

89

CU-186-68-ONR-266-Phys.

Hudson Laboratories
of
Columbia University
Dobbs Ferry, New York 10522

Technical Report No. 158

SUMMARY REPORT, ATMOSPHERIC PROPAGATION BACKGROUND STUDIES UP TO SEPTEMBER 1, 1968

by

Ivan Tolstoy, T. Herron, E. Bendor, and D. W. Kraft

UNCLASSIFIED

September 1968

This report consists
of 88 pages

Copy No 20
of 110 copies

This work was supported by the Office of Naval Research and the Advanced Research Projects Agency under Contract Nonr-266(84). Reproduction in whole or in part is permitted for any purpose of the United States Government.

ABSTRACT

After a brief description of the system, a summary is given of significant results obtained in describing properties of background pressure fluctuations in the Dobbs Ferry area. Particular emphasis has been given, during the last year or so, to understanding the effect of the tropospheric jet stream. It is shown, among other things, that a good part of this effect is probably due to the generation of internal gravity waves by the wind structure near the 300 mbar level. This mechanism is sensitive to wind shears. Finally, although the exact importance of stability waves in this picture is hard to ascertain as of now, a preliminary investigation of one class of stability waves is reported.

TABLE OF CONTENTS

BLANK PAGE

I. INTRODUCTION:

THE HUDSON LABORATORIES MICROBAROGRAPH ARRAY

In late 1965 the development of an ultra-low frequency (10^{-4} Hz < f < 1 Hz) microbarograph array was undertaken at Hudson Laboratories of Columbia University. Since we desired to include periods up to 90 min or so, we had to make our own microbarographs. This was done during the fall of 1965 and early 1966, following a design suggested and already partially tested by J. Young and R. Cook of the ESSA infrasonics groups in Washington, D. C. Further information concerning the microbarographs will be found in a report by Clay and Kraft.[1] Since 1966, the number of sensors operating in the field has varied between 1 and 16, depending upon the particular experiment being conducted. On the whole, the system has steadily grown to its present size of 16 microbarographs. A map showing the distribution of sensors as of spring 1968 is given in Fig. 1.

In addition to the microbarographs, the system includes one Doppler-shift type ionosounder and magnetometers at the Catskill (New York), Thornhurst (Pennsylvania), and Lebanon (New Jersey) sites.

All instrument outputs are transmitted by telephone lines to the central recording station at Hudson Laboratories in Dobbs Ferry. The data are recorded in digital form (BCD) on magnetic tape, with a total capacity of 32 channels capable of recording one four-digit number each twice a second ($\simeq$ 900 bits/sec^{-1}).

Most of the system's work to date has been oriented toward a study of background pressure fluctuations for periods of 5 min to 90 min, approximately. Velocities of propagation for naturally occurring disturbances in

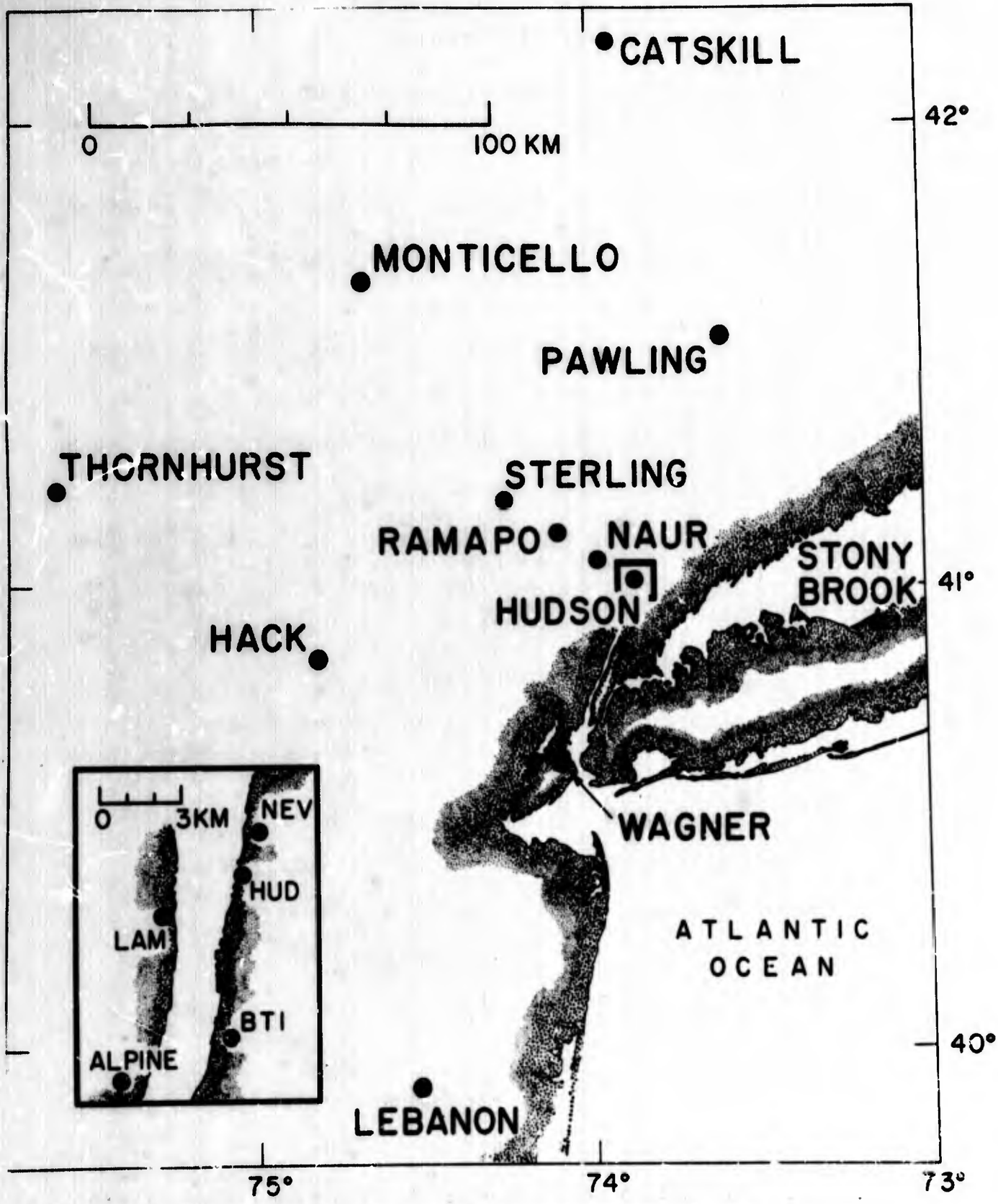

Fig. 1. Locations of microbarograph stations.

this band appear to vary from about 10 m sec^{-1} to several hundred m sec^{-1}. The corresponding wavelengths therefore vary from a few km to 10^3 km or so. This scale of dimensions corresponds to what the meteorologists refer to as the mesoscale, somewhere between meteorological phenomena proper at one end and boundary layer turbulence and wind effects at the other (micrometeorological effects, see, e.g., Lumley and Panofsky[2]). Insofar as the acoustician is concerned, periods $1 \text{ sec} \leq T \leq 10 \text{ min}$ are in the infrasonic domain. Periods $T > 10$ min , when they do correspond to wave phenomena, belong to the internal gravity wave part of the spectrum.

The spectral distribution of the background energy given by our studies is typified by the average, smoothed, type of behavior shown in Fig. 2. This particular curve is an average over many weeks of data. It is representative of hundreds of curves of this type obtained by us over a period of about two years. It is also consistent with earlier results of Gossard,[3] Golitsyn,[4] and Pinus et al.[5]

As a result of studies performed in the summer and fall of 1967, using the small scale network of microbarographs shown in the inset of Fig. 1, we have succeeded in showing quite conclusively that much of the energy input into this band comes from the jet stream. Thus, for lengthy periods of time (often for weeks on end) the direction of travel of pressure perturbations in this part of the spectrum closely follows that of the jet-stream winds aloft. The velocities of propagation, in the 20 - 50 m sec^{-1} range are also of the same order. In addition, preliminary calculations indicate that the correct order of magnitude for ground-level pressure perturbations, as well as the main spectral characteristics, are obtained if one assumes that the wind fluctuation power spectrums obtained from flying aircraft[6, 7]

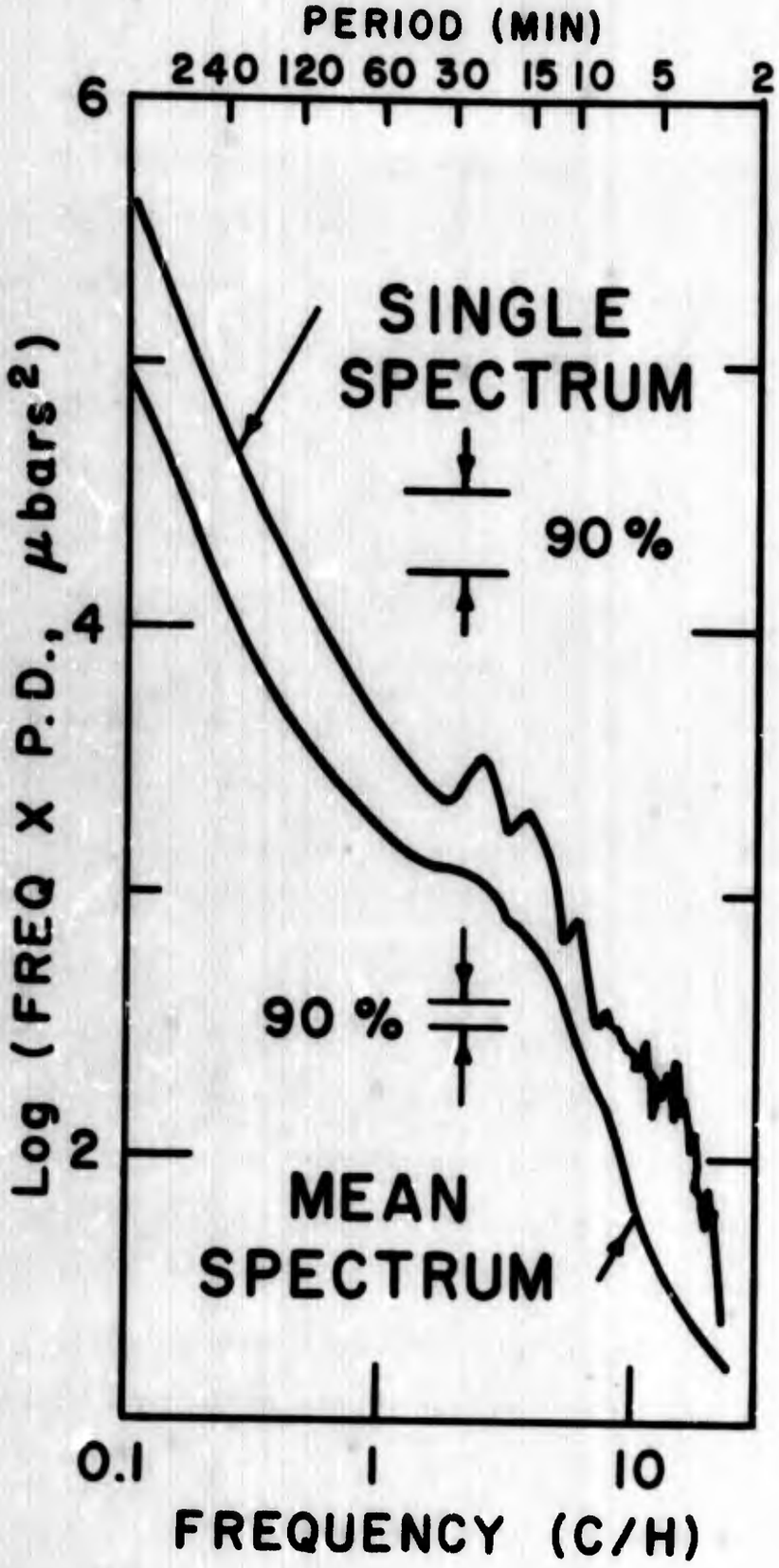

Fig. 2. Single atmospheric pressure power spectrum (24-hour sample of data, August 3, 1967) and mean of 27 single spectrums (from August 1967) for Hudson Laboratories station. The power density values were multiplied by the corresponding frequency in order to flatten the spectrums. The 90% confidence limits are shown for the single and mean spectrums.

correspond to internal gravity wave systems being shed by the jet stream. This mechanism not only yields the correct orders of magnitude for the pressure fluctuations, but also appears to explain the typical knee appearing on all pressure power spectrums in this band of periods.

Insofar as larger scale phenomena are concerned, the use of beam-forming techniques on the full array of Fig. 1 indicates the existence of disturbances having periods of 15 to 50 min, traveling at speeds in the 100 - 600 m sec^{-1} range. A systematic study of these processes is underway. If this is a wave phenomenon, as appears probable, then one is dealing with internal gravity waves of wavelengths between 300 and 1000 km.

Apart from long wavelength internal gravity waves of this type and short wavelength ones of the kind generated by the jet stream, there exist other processes for the propagation of pressure disturbances in the meso-scale range. Obvious candidates are wind-borne convection systems, large-scale eddies, etc. There is also another fairly obvious wave phenomenon, i. e., that of stability (or instability!) waves in shear flows. This type of disturbance is well known to hydrodynamical theorists (see, e. g., Lin[8]). Clearly the tropospheric wind system which culminates in the jet stream at 10 km altitude represents a steady shear flow capable of supporting waves of this kind. A more thorough theoretical and experimental study of the relevance of these waves is desirable.

II. ANALYSIS PROCEDURES AND GENERAL PROPERTIES OF THE PRESSURE FLUCTUATION BACKGROUND

Various sources of mesoscale pressure fluctuations are known, such as mountain lee waves, convective activity, gravity waves on inversion surfaces in the lower troposphere,[3, 9, 10] acoustic-gravity waves generated by thunderstorm activity,[11] and disturbances associated with tropospheric jet streams.[12-15] The contribution of any of these mechanisms to the total pressure variance depends, of course, upon the geographic area. In the New York area, the largest mesoscale pressure fluctuations are disturbances which move with weather fronts at about the same speed as the frontal movement (10-15 m/sec). The slow movement of a storm area across the array is easily identified; the fluctuations are often coherent over many tens of kilometers. However, in the absence of storms there is still a continuous lower-level background fluctuation which is also a major contributor to the mesoscale pressure spectrum. Through the use of power- and cross-spectral techniques, the spectral characteristics, spatial coherence, and origin of the major portion of background noise are described.

The microbarographs used for measuring the pressure variations were built at Hudson Laboratories[1] to provide the sensitivity and frequency response required for this program. They are high-pass instruments that compare the pressure of the atmosphere to the pressure in a reference volume. The reference volume is connected to the atmosphere by a "leak," which is adjustable, allowing the long period response of the instrument to be varied. A transducer responding to differential pressure provides a

voltage output for measurement. The microbarographs were calibrated by measuring their response to a step function in pressure. The step and rate of decay give the amplitude calibration constant and high-pass time constant. They were adjusted to have a flat frequency response from a 1-sec to about a 10-min period. At longer periods, the response falls off at 6 dB/octave, thus providing some spectral prewhitening against a background power spectrum which rises steeply toward long periods.

A microbarograph found to have a very stable phase response during initial testing was installed at Hudson Laboratories and designated a standard against which other field microbarographs were compared. A very accurate, but relative, amplitude and phase calibration of the instruments is obtained by digitally recording the broadband atmospheric pressure background noise as measured simultaneously by both the field and standard instrument. A cross-spectral analysis of the two microbarograph outputs, for 24-hour samples, then provides the relative amplitude and phase response for periods up to several hours. The coherence figure given by the cross-spectral analysis is a sensitive indicator of the stability, with time, of the relative phase response. Repeated tests of microbarographs over several weeks showed that their phase response is stable to ±4 or 5 degrees from the Nyquist period to 1- or 2-hour periods. At longer periods, the phase stability begins to degenerate due to thermal changes in the reference volume. However, a high degree of thermal insulation and operation at temperature-controlled sites provide reliable data at periods as long as several hours.

Data are transmitted over the array in both analog and digital modes. Three stations (Lebanon, Thornhurst, and Catskill) are the sites of digital

transmission links (8 channels each) to a master station at Hudson Laboratories where there is a fourth 8-channel digital input unit. Pressure data from other stations of the array are transmitted as frequency-modulated analog signals to the nearest digital link to Hudson Laboratories. At Hudson Laboratories the digitized data (up to 32 channels) are multiplexed and recorded on magnetic tape with accurate time information. Sampling intervals of the digital system can vary from 1 to 10 sec.

The instrument noise levels of the microbarographs and of the data transmission recording system were measured and found to be much lower than the atmospheric noise levels which were to be investigated. The over-all system resolution is approximately 5 μbar. The filter response of the entire system (for a 10-sec sampling interval) is shown in Fig. 3.

Computer programs were written to convert the raw digital data into edited data, free of digitizing errors. All edited data were played back on a digital plotter and checked visually for fidelity to the original signals, which were also recorded in analog form.

Power spectrum analyses were performed by the method of Blackman and Tukey.[16] The spectrum of atmospheric pressure variations rises at approximately 7 dB/octave toward the long periods.[3] Prewhitening of the spectrums is necessary to avoid "leakage" of energy into the spectral band of low power. However, the high pass microbarographs did not adequately flatten the spectrums so an additional prewhitening was applied by a digital filter. A maximum lag of 8% of the record length was used in the autocorrelation. A hanning window was used to smooth the raw spectrums and the spectrums were then restored to compensate for the effects of the analog and digital filters. The power density was computed in units of microbars squared per cycle per hour. For presentation in this report, the power density estimates have been multiplied by the

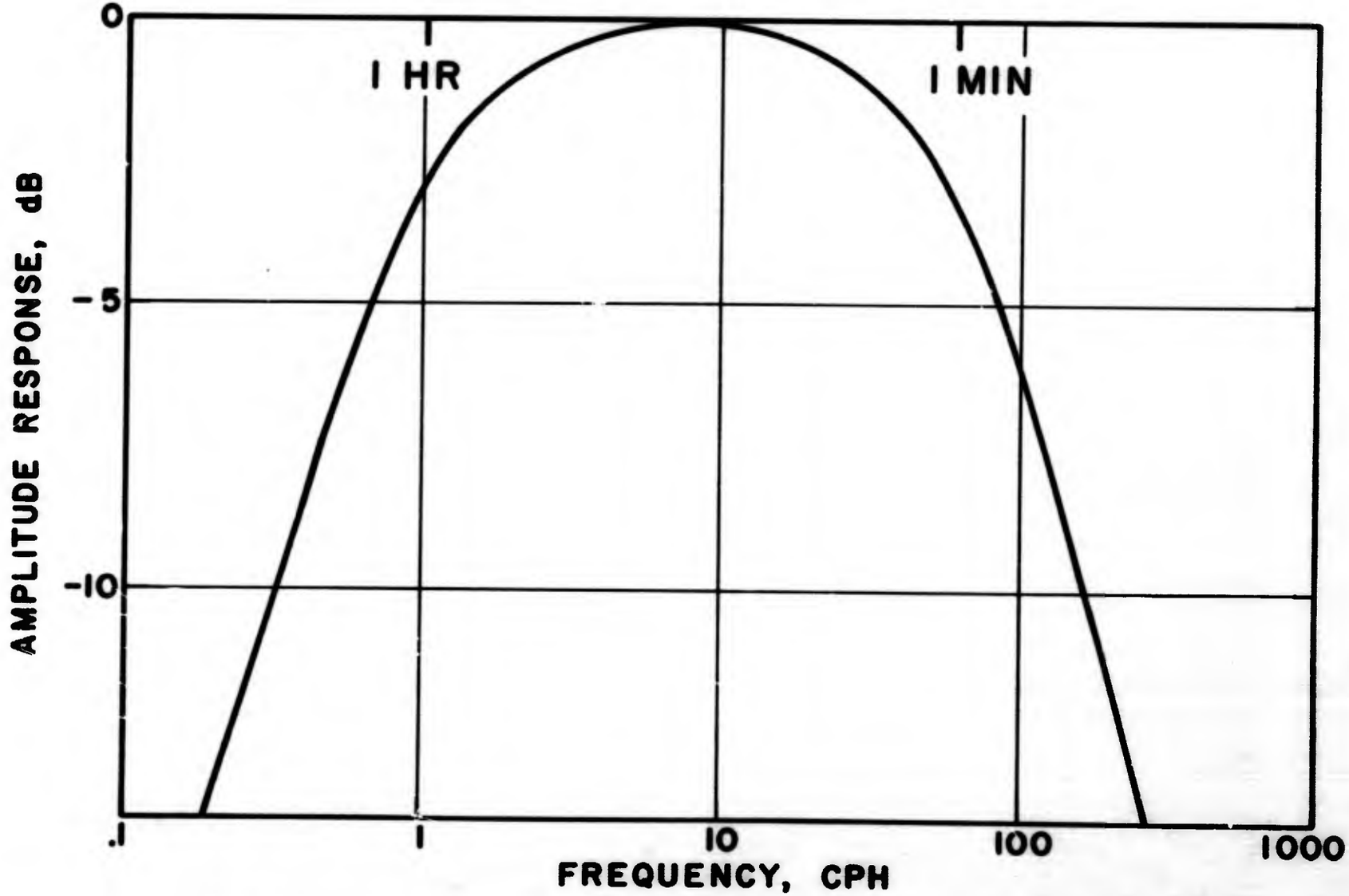

Fig. 3. Filter characteristics of the transducer-data-recording system. The low-frequency cutoff is controlled by the "acoustic" filter of the microbarograph. The high-frequency cutoff is controlled by an electrical filter at the input to the digital system, and is adjusted to the sampling rate to prevent aliasing.

corresponding frequency which has the effect of flattening the spectrum. The log of frequency times power density is plotted versus the log of frequency.

Cross-spectrum analyses were performed upon pairs of microbarograph signals to yield phase angles and coherencies between the signals. For these analyses the data were treated in a manner similar to that described for power spectrum analyses; in addition, the phase angles were corrected for the phase shifting effect of the instrument filters.

In order to search the records for intervals of high coherence and to measure any motion of the pressure fluctuations, a "moving" cross-spectrum analysis computer program was developed in which a "time window" was moved across a set of signals in overlapping steps. Within each "time window" cross-spectrum analyses were performed between various pairs of signals in the set. The time at the center of the "window" was assigned to each coherence and phase angle measurement. By this method, the data could be searched for time intervals of high coherence across the array. The geometry of the array was given to the computer and when a coherence across the array above a specified value was found for any frequency band, the apparent phase velocity vectors between stations were computed. A least-squares fit of a straight line through the tips of the vectors then gave the orientation of an assumed plane wavefront. Thus estimates were obtained of the true speeds and directions of pressure fluctuations moving coherently across the microbarograph array.

A. Temporal Characteristics of Noise Spectrums

Beginning in January 1967, power spectrums of contiguous 24-hour sections of records were computed for several stations of the array. Figure 4 shows a superposition of 25 spectrums for the Hudson station for the month of September 1967. The typical variability of the individual spectrums is seen in a spread of more than an order of magnitude in power density. To eliminate the variability and reveal statistically stable features, the spectrums from each station were averaged for each month to yield mean monthly spectrums. Figure 5 shows the mean monthly spectrums for Hudson for the year 1967. Each monthly spectrum is the mean of at least twenty 24-hour spectrums. Figure 5 summarizes the spectral characteristics of over 220 days of atmospheric pressure fluctuations for periods of 3 min to 10 hours. At periods shorter than 3 min a single dotted curve is shown. This curve is a mean of 22 spectrums of one and one-half hour records from various stations of the array. These 33 hours of data were recorded at scattered intervals during daylight hours in July 1967. The dashed curves of Fig. 5, enclosing the mean spectrums, are envelopes of the extreme spectrums included in the mean curves.

The seasonal variation of the pressure spectrum for various period bands is shown in Fig. 6. Over a broad range of periods, from 3 min to 10 hours, the spectrum levels are from one-half to a full order of magnitude lower during the months of June through September, as compared to the highest levels of April and December.

Two features of interest in Fig. 5 are the "knees" in the mean spectrums between 1 and 10 cph and the peak at about 100 cph in the single short

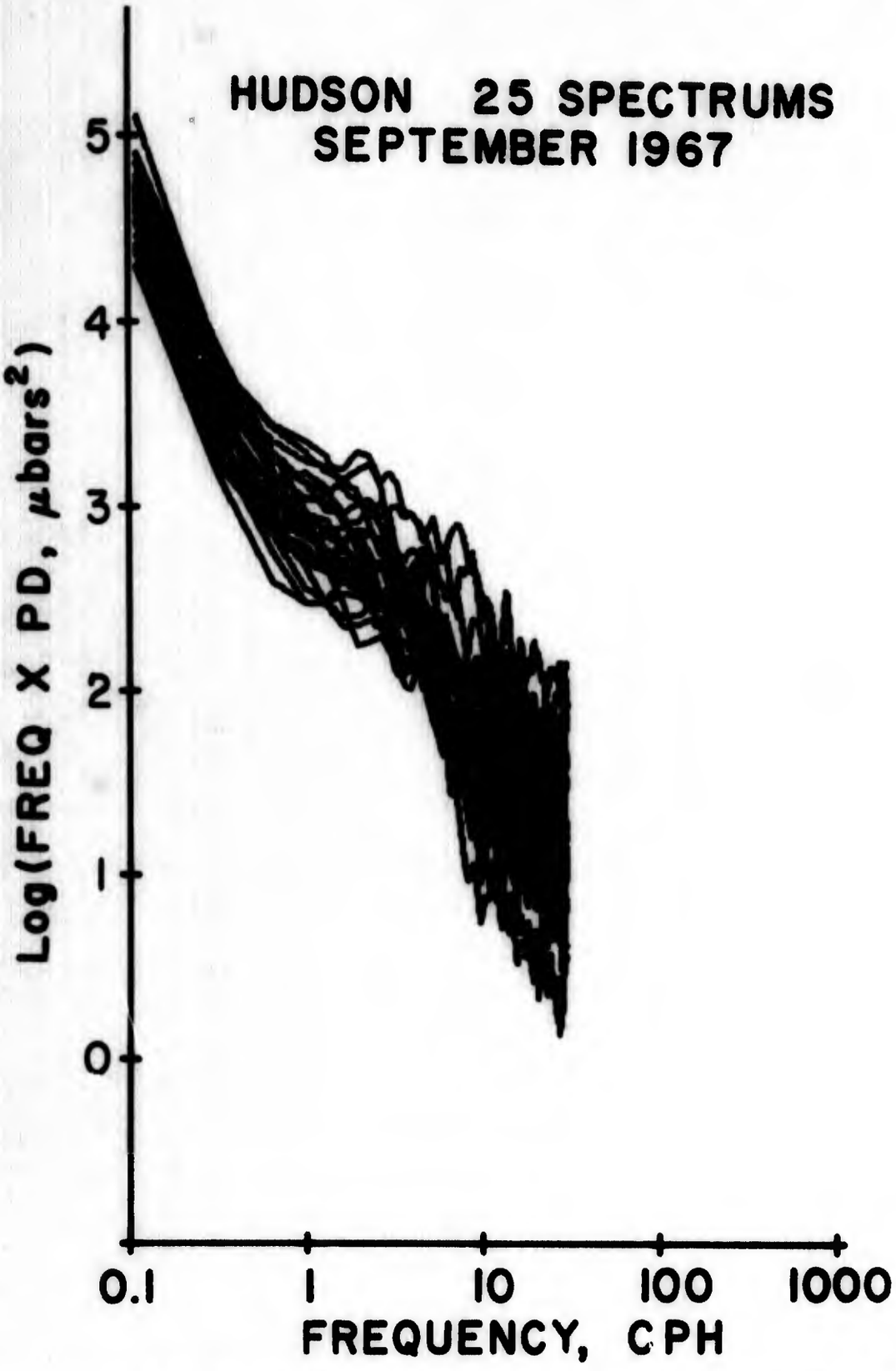

Fig. 4. Pressure spectrums of 24-hour samples of data.

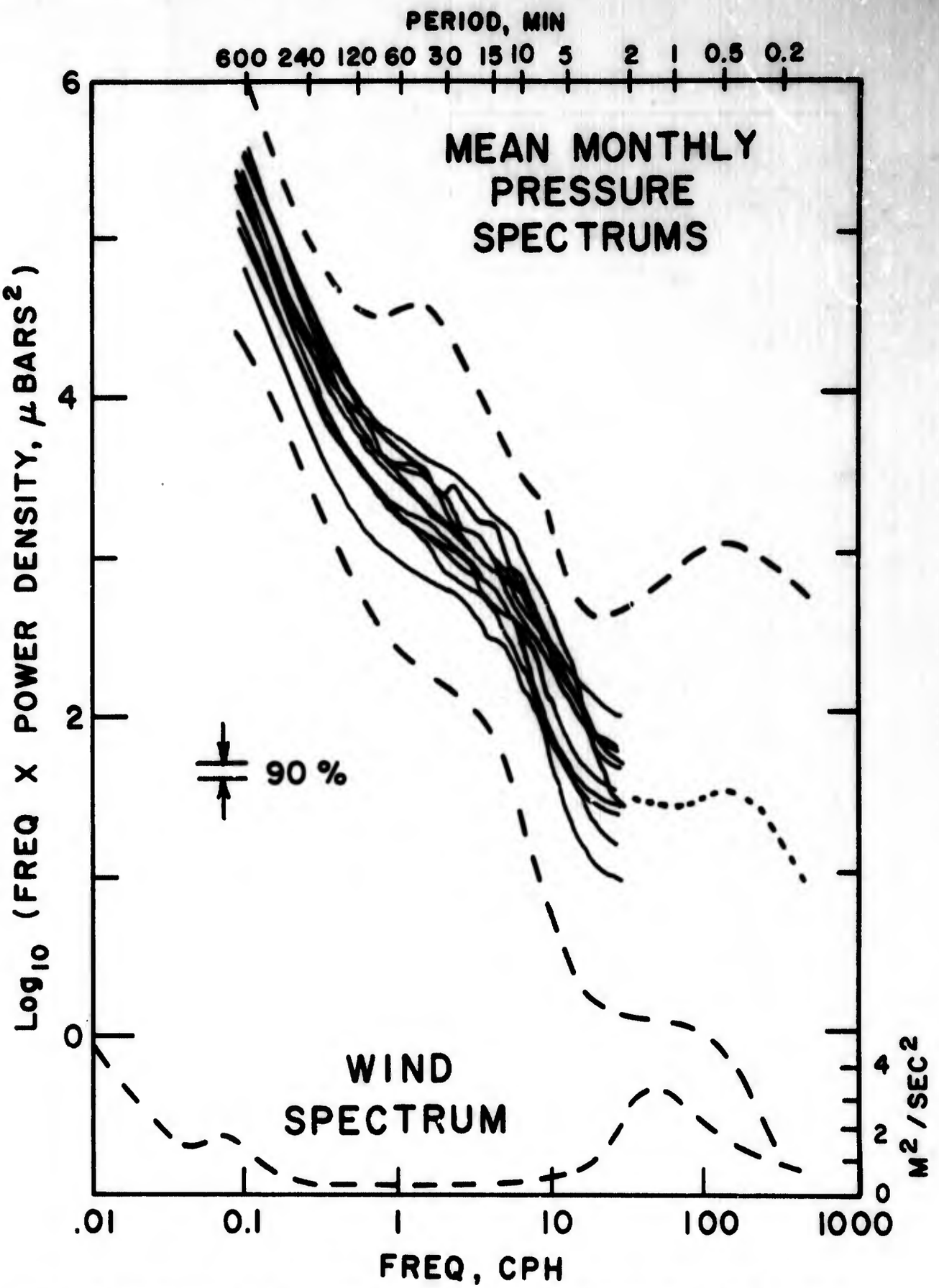

Fig. 5. Mean monthly pressure spectrums of 24-hour samples of data, from the Hudson Laboratories station, for the year 1967. The single dotted curve at high frequencies is a mean of July data. The dashed lines indicate the extreme spectrums included in the means. The wind velocity spectrum of Van der Hoven [17] is shown at the bottom. The bars give the 90% confidence limits of the mean spectrums.

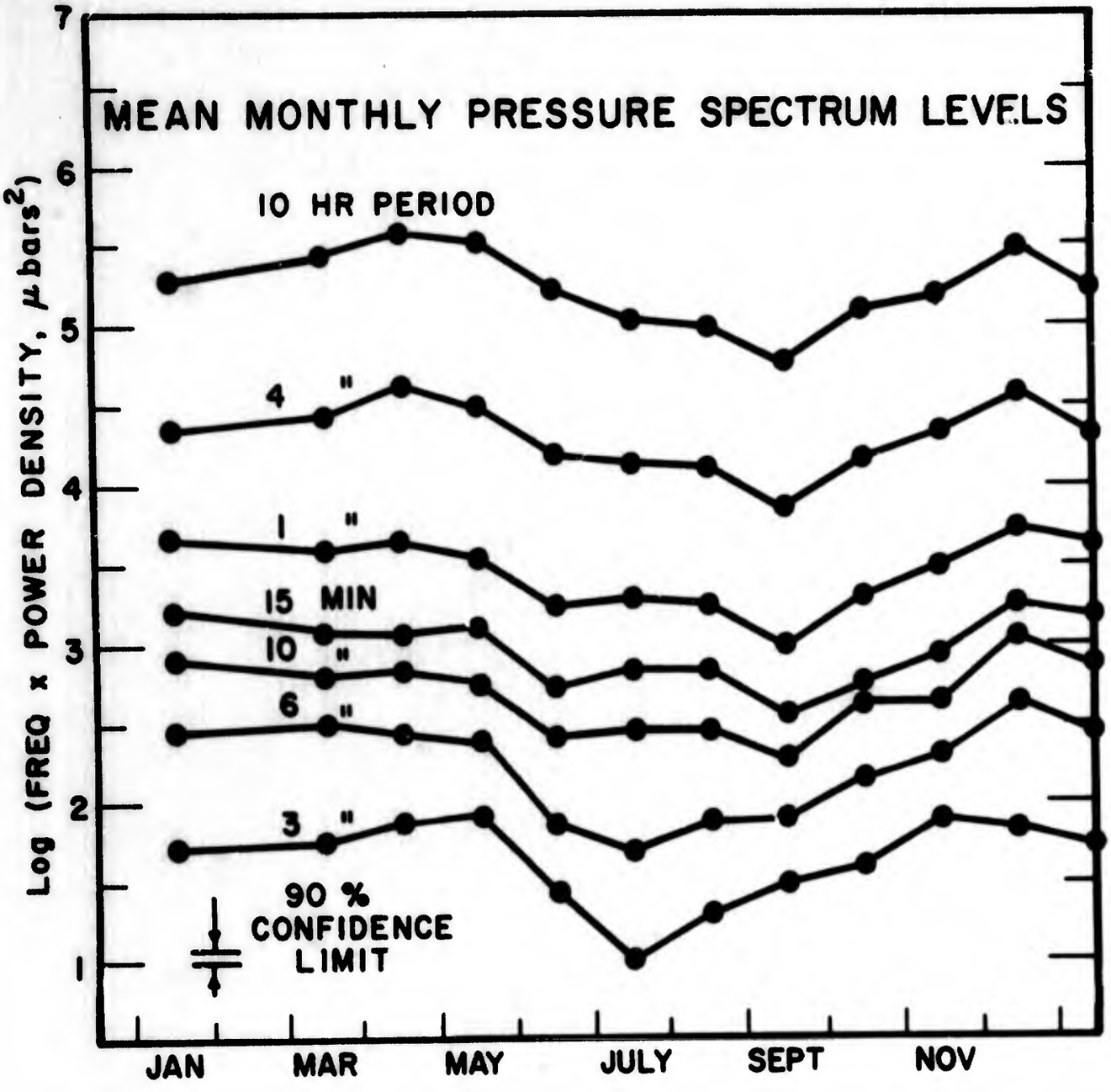

Fig. 6. Seasonal variation in spectrum levels. The mean values were assigned to the middle of the month. February is missing due to inadequate data.

period mean spectrum. These features of the mean spectrums are accompanied by widening of the spectral envelopes, indicating greater variability of the individual spectrums in these bands.

The short period peak in the pressure spectrum results from turbulence effects at the earth's surface. It is known to correlate[3] with a corresponding peak in the wind velocity spectrum of Van der Hoven,[17] shown as a dashed line at the bottom of Fig. 5. The short period correlation is a micrometeorological phenomenon. A point of separation between short period phenomena and longer period, mesoscale phenomena was investigated, for the topographic conditions prevailing in the Hudson Laboratories area, by making simultaneous measurements of wind and pressure and computing power densities of the pressure for different wind states. An additional microbarograph was operated at the base of a 100-m tower near Alpine, New Jersey, while wind speed was recorded at the top of the tower. The tower is in a wooded area 1 km from a 120-m cliff overlooking the Hudson River. Power densities of thirty-six 2- to 3-hour sections of record were then correlated with wind speed averaged over the same time intervals. The log of power density correlated linearly with wind speed. Figure 7 shows the correlation coefficient versus period. The correlation is a maximum at 10- to 50-sec periods, decreasing rapidly beyond the 2-min period. In the range of maximum correlation, power density, in microbars squared per cycle per hour, varied with wind speed, v, in meters per second, approximately as

$$\text{P.D.} = 0.0025\, e^{0.89v}$$

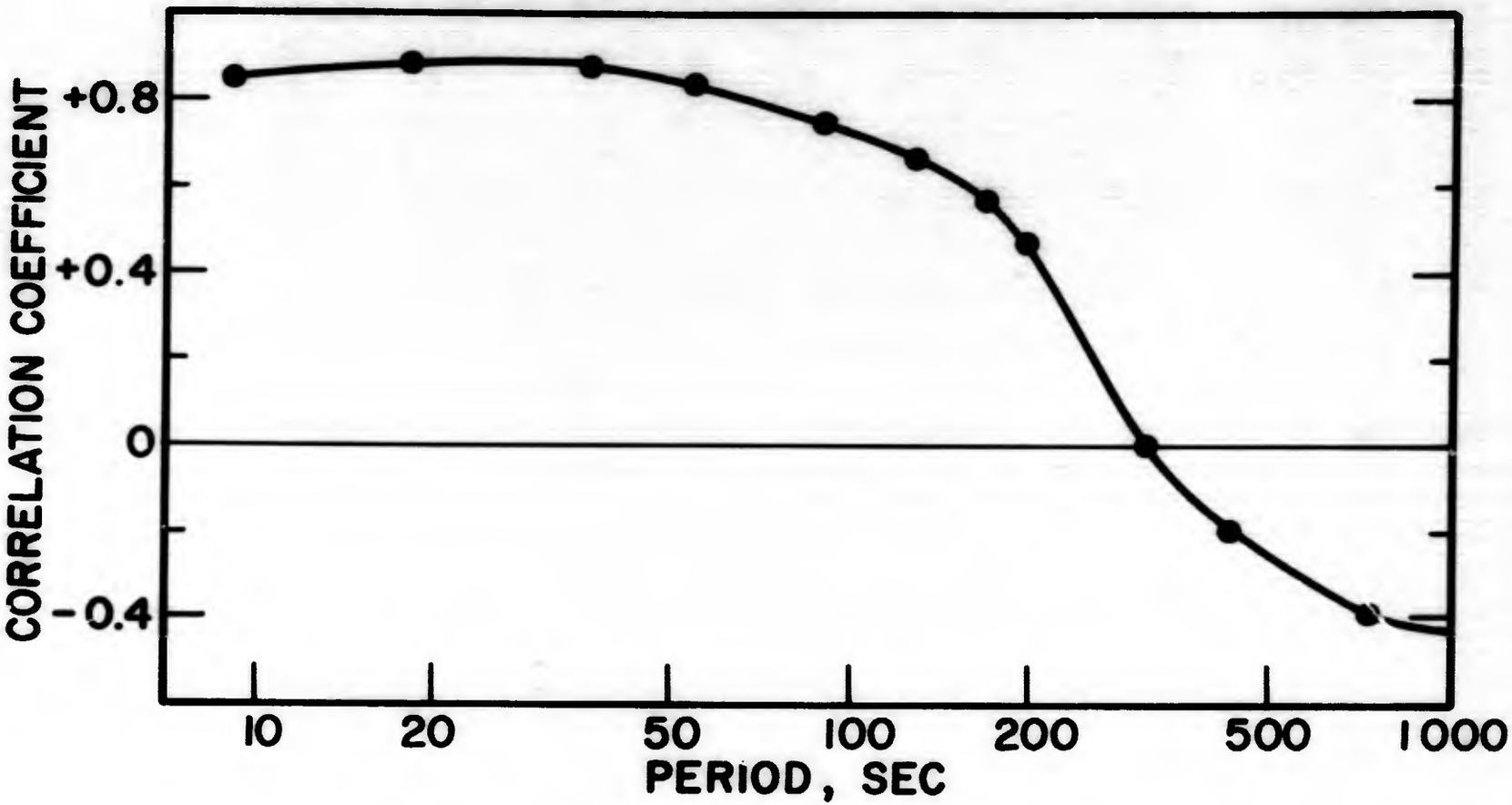

Fig. 7. Linear correlation coefficient of the logarithm of ground-level power density of pressure variations with wind speed at 100 m.

These results agree generally with the spectral properties reported by other authors. Gossard[3] presented a broadband spectrum and discussed its character. Golitsyn[4] described short period spectrums, pointing out the minimum at 1- to 2-min periods. Figure 5, however, summarizes far more spectral information than has previously been available and provides statistically reliable information concerning seasonal changes in spectral activity.

B. Spatial Characteristics of Noise Spectrums

Figure 8 shows plots of the mean spectrums for May and September 1967 at several stations separated by tens to hundreds of kilometers. Over the entire mesoscale period range, the spectrums at these stations are very similar in shape and level, at least as compared to the wide range of daily spectrums at any one station (Fig. 4). There is an indication, from Fig. 8, that over large distances spectral levels are more nearly equal at the long periods.

The spatial coherence of the background noise was studied by computing cross-spectral coherencies of 6-hour sections of simultaneous records for 11 pairs of stations at separations ranging from 1.4 to 36 km. The coherencies were found to decrease approximately as the log of distance for period bands of 8 to 64 min (Fig. 9). The 8-min curve flattens out at a coherency level of about 0.1, which is a level of "random" coherence. Similar computations for 4- and 24-hour samples of data showed nearly the same coherence levels versus distance.

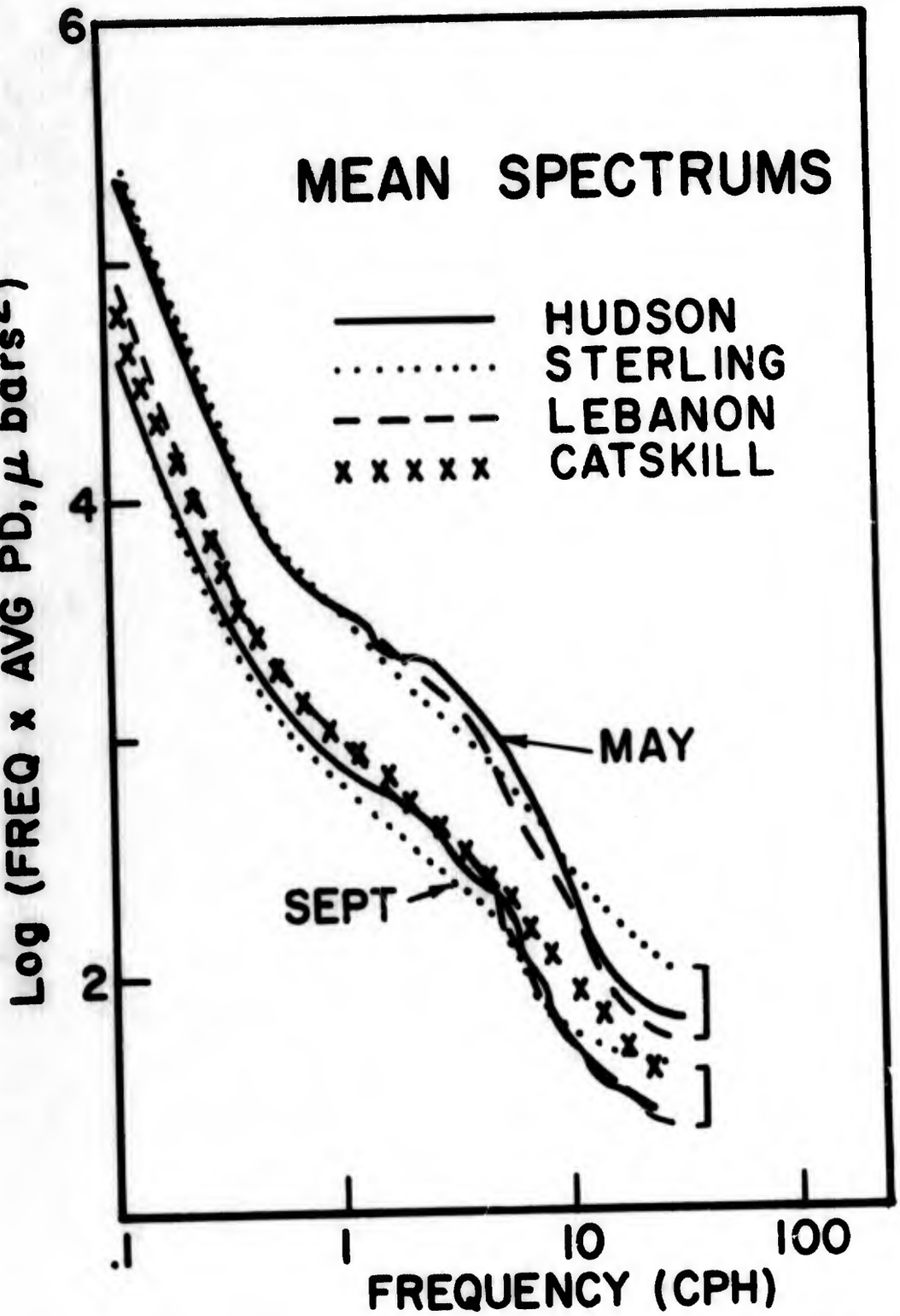

Fig. 8. Comparison of mean monthly spectrums at various stations of the microbarograph array.

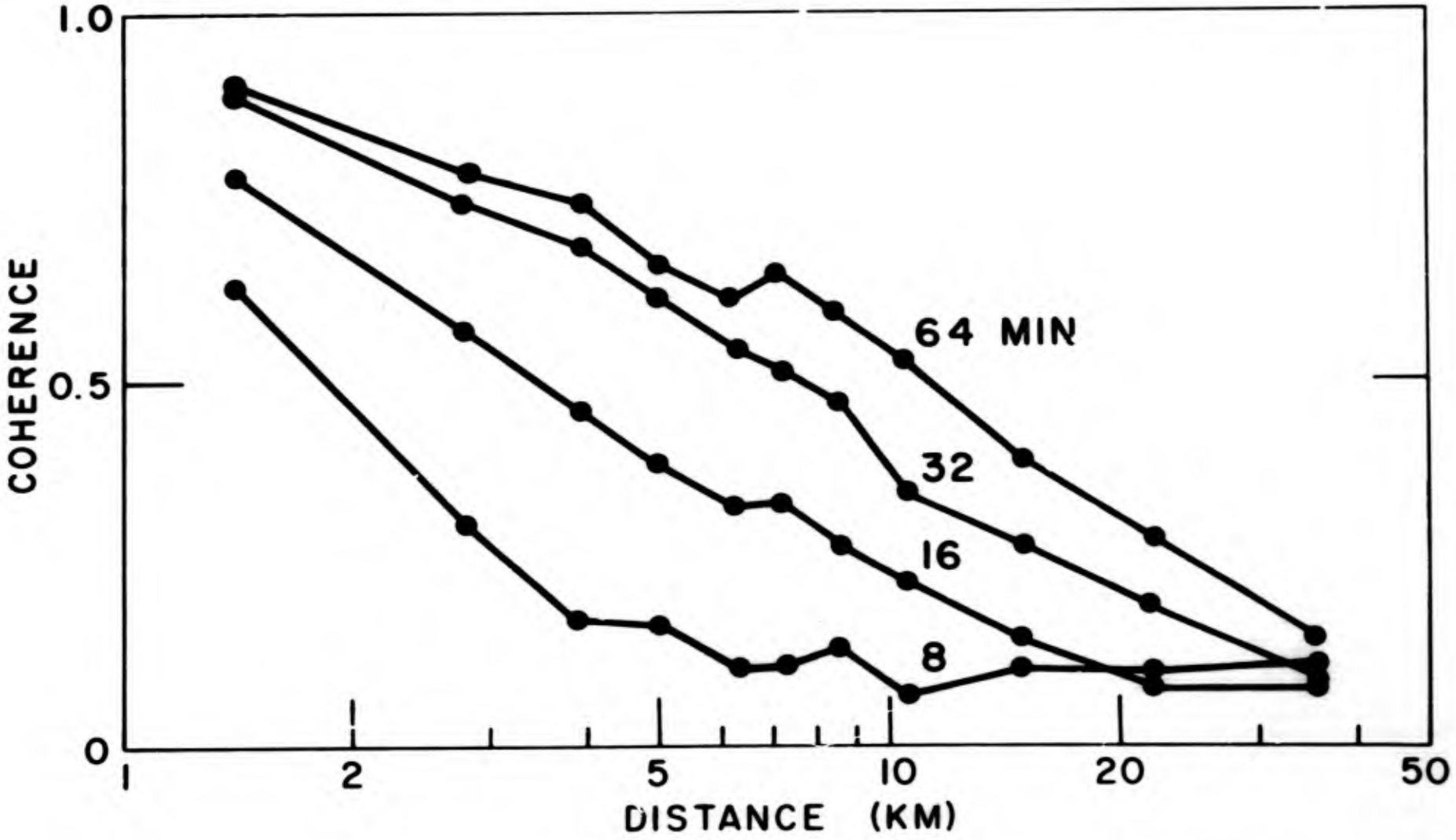

Fig. 9. Mean cross-spectral coherencies of forty 6-hour samples of simultaneous data from 11 pairs of stations. The data were scattered throughout November and December 1967.

C. Movement of Noise across Array

The "moving" cross-spectral analysis was applied to data obtained from the small array of a few kilometers spacing. Using 4- and 8-hour "time windows" for the analysis, it was found that much of the background noise in the 20- to 90-min period range moved coherently across the array, generally from the west at speeds of 10 to 50 m/sec. Figure 10 shows background noise observed on the small array. Figure 11 is a polar plot of the directions from which the pressure fluctuations of Fig. 9 move. Figure 11 also indicates the direction of jet-stream winds over Hudson Laboratories as determined from U. S. Weather Bureau maps of tropopause winds. A study of many weeks of data, by this method,[18] showed that most of the background noise moved across the array with directions and speeds that correlated with the jet-stream winds.

D. Correlation of Spectrum Levels with Upper Wind Velocities

The association of mesoscale background noise with the upper winds was further investigated by attempting a correlation of pressure spectrum levels with the maximum tropospheric wind velocity over Kennedy Airport, the nearest station (35 km) to Hudson Laboratories at which wind measurements are made. Spectrum levels were computed for 10-hour samples of microbarograph data, for the period band of 40 to 120 min. Data collected from August to October 1967 were used. Spectrums of large pressure fluctuations caused by the passage of storms were excluded. Figure 12 shows the resultant correlation to be rather weak.

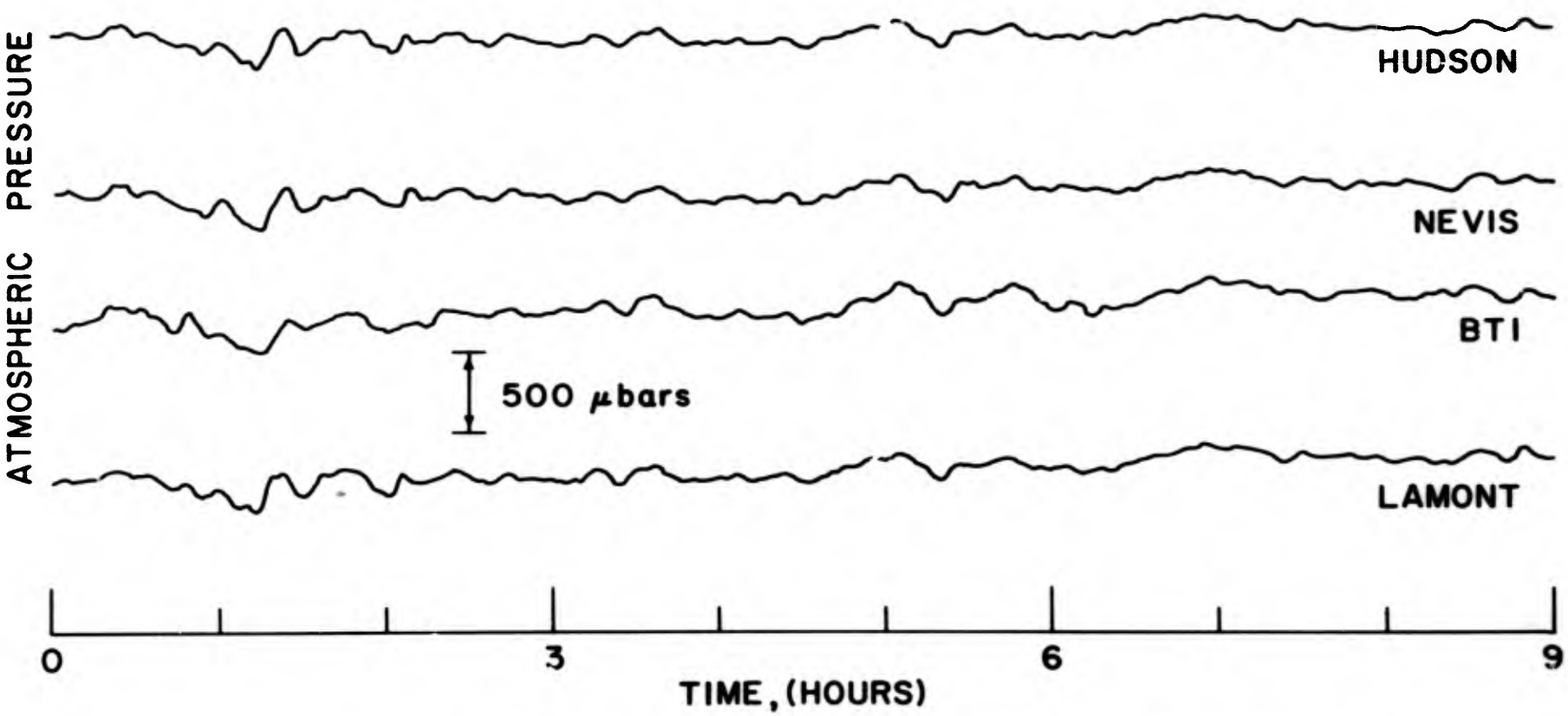

Fig. 10. Example of pressure fluctuations generated by jet-stream winds. The coherence of the fluctuations at stations separated by several kilometers is easily seen. The data are from October 14, 1967.

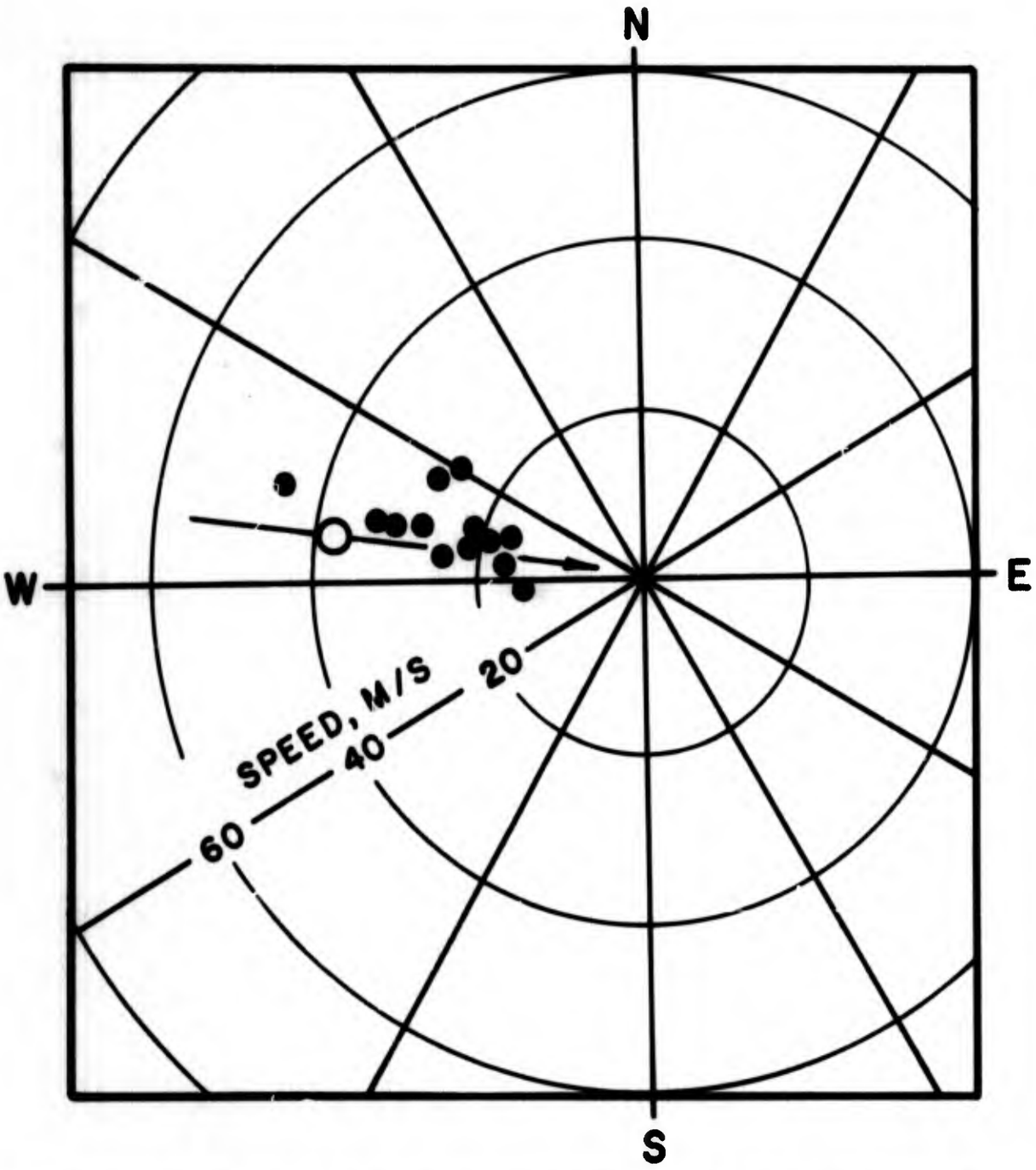

Fig. 11. Directions and speeds of propagation of the pressure fluctuations of Fig. 10. The directions were determined by a "moving" cross-spectral analysis using a 4-hour "time window." The solid points give the directions of propagation of fluctuations of 16- to 48-min periods, during a 12-hour interval on October 14, 1967. The open circle gives the direction of the jet-stream winds over the array, during the interval.

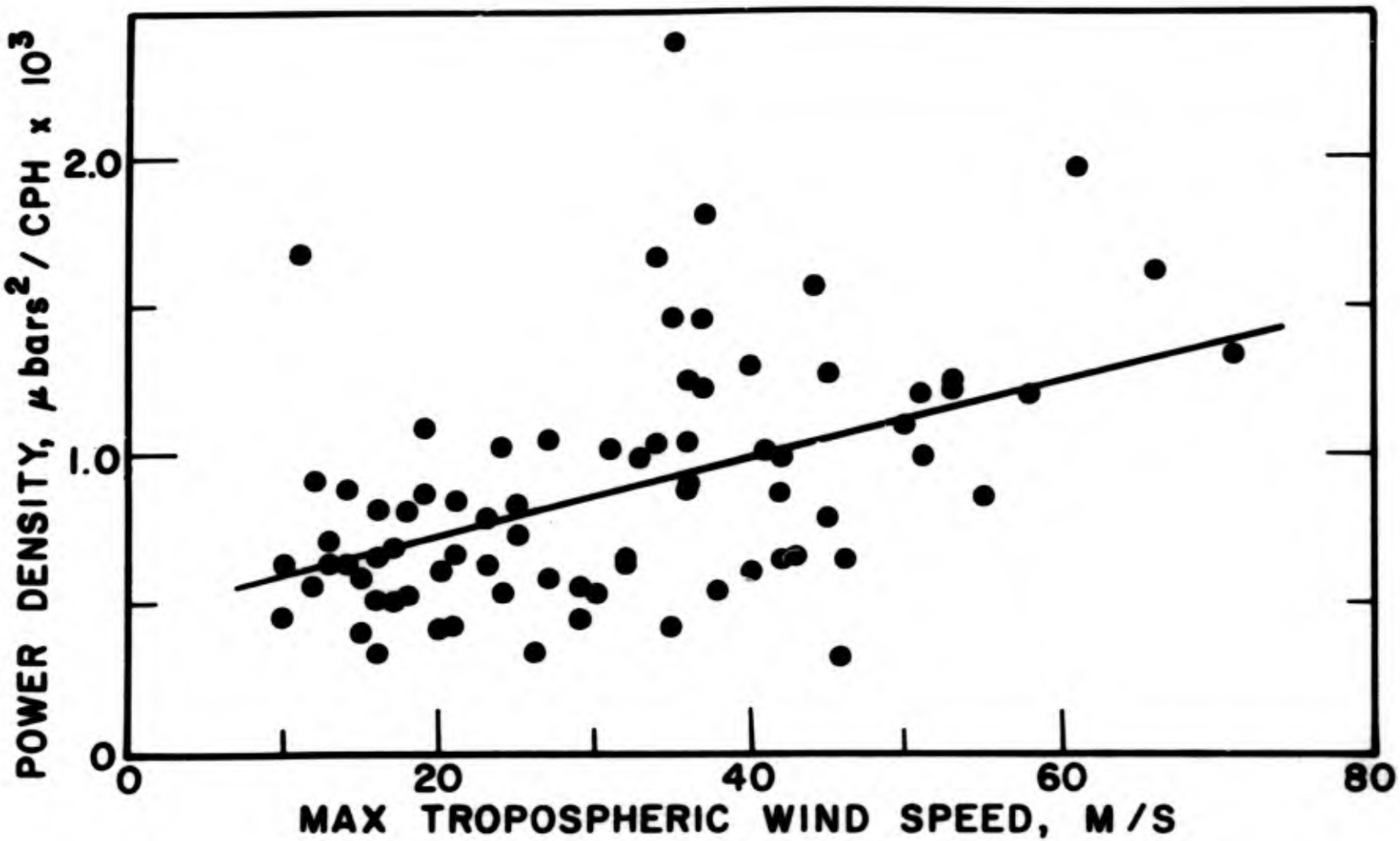

Fig. 12. Correlation of ground-level pressure fluctuation power densities at Hudson Laboratories with the maximum tropospheric wind speed at Kennedy Airport (35 km distant).

E. Discussion

The knee in the mean spectrums and the greater variability in the individual spectrums (Fig. 5) identify the 1- to 10-cph range as a spectrum band of energy input to the lower atmosphere. The spectrum levels in this mesoscale range were observed to vary with season (Fig. 7). In the mid-latitudes, where weather conditions are controlled by the behavior of the polar-front jet stream, it is reasonable to consider the jet stream as a source of seasonal variations in the mesoscale pressure spectrum. Kao and Hurley[19] presented graphs of the monthly horizontal positions of the cores of maximum mean kinetic energy of the jet stream and of maximum turbulent kinetic energy associated with the jet stream. Correlation of seasonal spectrum levels with the horizontal distances of these cores from Dobbs Ferry showed best correlation with the core of maximum velocity. The data of Kao and Hurley show that the region of maximum velocity over the northeastern United States passes over Dobbs Ferry in the months of April and December, the same months for which the pressure spectrum levels (Fig. 6) at Dobbs Ferry are highest. The region of maximum velocity is most remote from Dobbs Ferry in June through September when the levels are lowest. The more recent data of Kao and Farr,[20] however, seem to indicate that the spectrum levels may correlate better with the core of maximum turbulent kinetic energy than with the core of maximum mean kinetic energy.

The question arises as to the mechanism by which the ground-level pressure spectrum is related to the tropopause winds. Consider first that the pressure fluctuations may result from processes associated with the passage of synoptic-scale weather systems. This would explain the seasonal

correlation of spectrum levels with the position of the turbulent core since Kao and Farr have shown that the principal cyclone tracks generally coincide geographically with the turbulent core. In support of this suggestion we do, in fact, observe that the greatest pressure variance occurs when storm centers move across the microbarograph array. In considering the exact process by which mesoscale pressure fluctuations result from synoptic-scale motions, it is unlikely that they are produced by wind fluctuations due to mesoscale eddies since Van der Hoven[17] has clearly shown a minimum in the mesoscale wind spectrum. An alternative possibility is that the pressure fluctuations result from waves generated by weather disturbances.

The above considerations relate the pressure spectrum to synoptic conditions which in turn relate to the position of the core of maximum turbulence. This would imply correlation of the spectrum levels with the upper winds on a monthly or seasonal basis.

There is also direct transmission of energy from the upper winds to the earth's surface. The experimental evidence for this statement is that much of the pressure background fluctuations on the array, other than storm activity, moved with directions that correlated on an hourly or daily basis, with the direction of the tropopause winds over the array at that time. This correlation sometimes persists for weeks (see section III). A mechanism by which the jet stream could put energy into the ground-level pressure spectrum is described in section IV, and consists of internal gravity wave excitation by perturbations of the jet. This mechanism predicts the correct order of magnitude of the mesoscale pressure spectrum and appears to be consistent with Van der Hoven's[17] observation of extremely low wind velocity variance in the mesoscale range.

The highest pressure spectrum levels (outlined in Fig. 5 by the upper dashed line) are representative of disturbances associated with weather fronts, while the mean spectrums are representative of jet-stream activity. Although the weather front disturbances contribute most to the pressure variance on a monthly average, they make the large contribution during relatively short intervals of time. In contrast, the jet-stream winds provide a fairly continuous, though lower-level, background.

III. TRACKING JET-STREAM WINDS BY GROUND-LEVEL PRESSURE MEASUREMENTS

The spectral properties of atmospheric pressure variations were studied by computing mean monthly power spectrums based on 24-hour samples of data as described in section II. Here we wish to draw attention to Fig. 2, showing the mean of 27 single spectrums at Hudson Laboratories for August 1967. Mean spectrums for other months are similar in shape. Also shown in Fig. 2 is one of the individual spectrums included in the mean. This spectrum contains fine structure, in the 1 to 10 cycles hr^{-1} range, which is typical of many of the individual spectrums. The fine structure is variable from spectrum to spectrum. It was also observed that the power levels of the spectrums were most variable in the 1 to 10 cycles hr^{-1} range. The mean spectrums were computed in order to average out the fine structure and the variability in spectral level and reveal statistically stable spectral features.

The knee in the mean spectrum and the greater variability observed in the individual spectrums in the 1 to 10 cycles hr^{-1} range indicate that there is energy input to the ground-level atmosphere in this spectral range. It was further observed that the mean monthly spectral levels varied throughout the year as the mean position of the jet-stream core moved relative to the Dobbs Ferry area, suggesting that the jet-stream winds are the major source of pressure fluctuations in the mesoscale range. The analysis to be described below confirms this hypothesis.

In general, the background noise showed nearly complete decorrelation at the station separations of the large array, but relatively high

correlation over the small array of Fig. 1 (section I). This noise coherence over the small array was utilized in a "running" cross-spectral analysis computer program which moved a "time window" in overlapping steps across the set of signals from the small array (Fig. 13). Within each "time window," cross-spectral analyses were performed between various pairs of signals of the set. The time at the center of the window was assigned to each coherence and phase angle measurement resulting from the cross-spectral analyses. By this method, disturbances moving across the array could be detected by searching for time intervals of high coherence. The geometry of the array was given to the computer and when coherencies above a specified value were found, apparent phase velocity vectors between stations were computed (Fig. 14). A least-squares fit of a straight line through the tips of the vectors then gave the orientation of an assumed plane wavefront. Thus measurements were obtained of the true speeds and directions of pressure disturbances, of various frequencies, moving across the array.

The result of applying this technique to several weeks of data in September 1967 is demonstrated in Fig. 15. The ground-level pressure disturbances moved generally out of the west and although the observations scatter over about 60° of azimuth, they very clearly correlate with the synoptic period changes in direction of the tropopause winds. The directions of the jet stream over Dobbs Ferry were interpolated from U. S. Weather Bureau tropopause wind maps.

The pressure disturbance directions of Fig. 15 were obtained by using both a 4-hour and an 8-hour "time window" and requiring a minimum coherence of 0.65 between signals for a speed-direction determination.

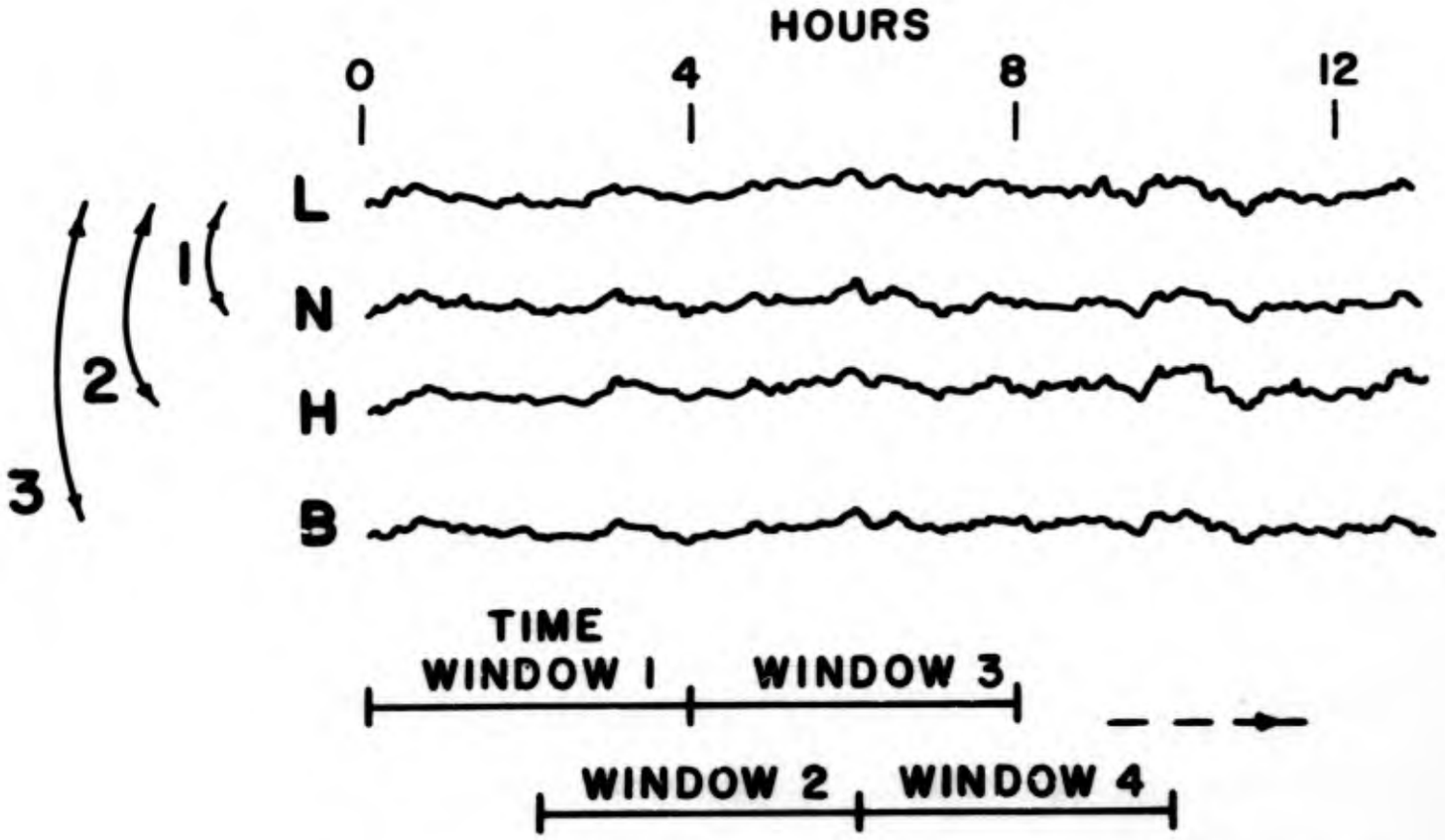

Fig. 13. Sample of atmospheric pressure background fluctuations caused by jet-stream winds. Within each "time window" cross-spectral analyses were performed between the Lamont data channel (L) and each of the other channels.

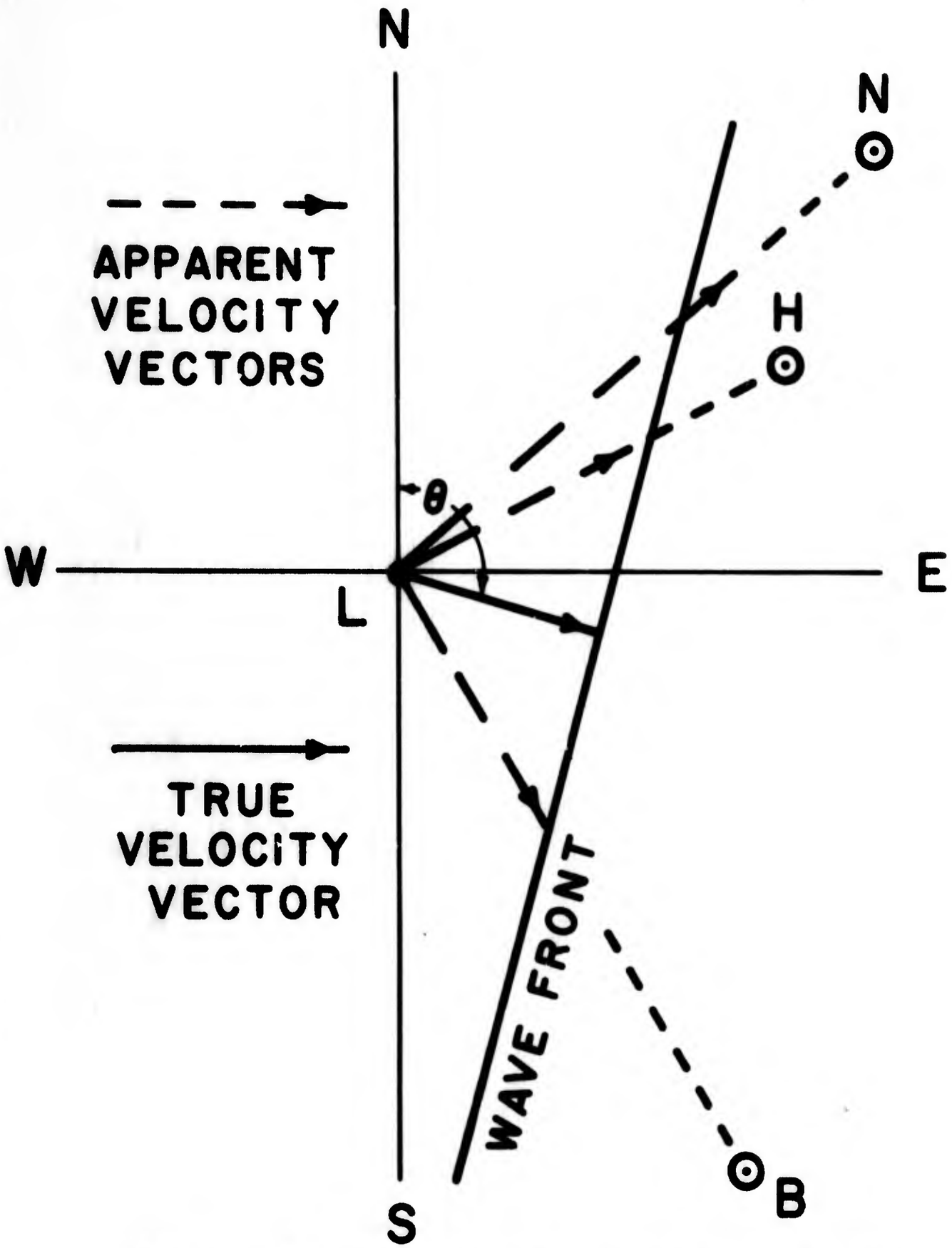

Fig. 14. Least squares fit of straight-line wavefront through tips of apparent phase velocity vectors resulting from cross-spectral phase measurements. Magnitude and direction of true velocity vector is given by computer.

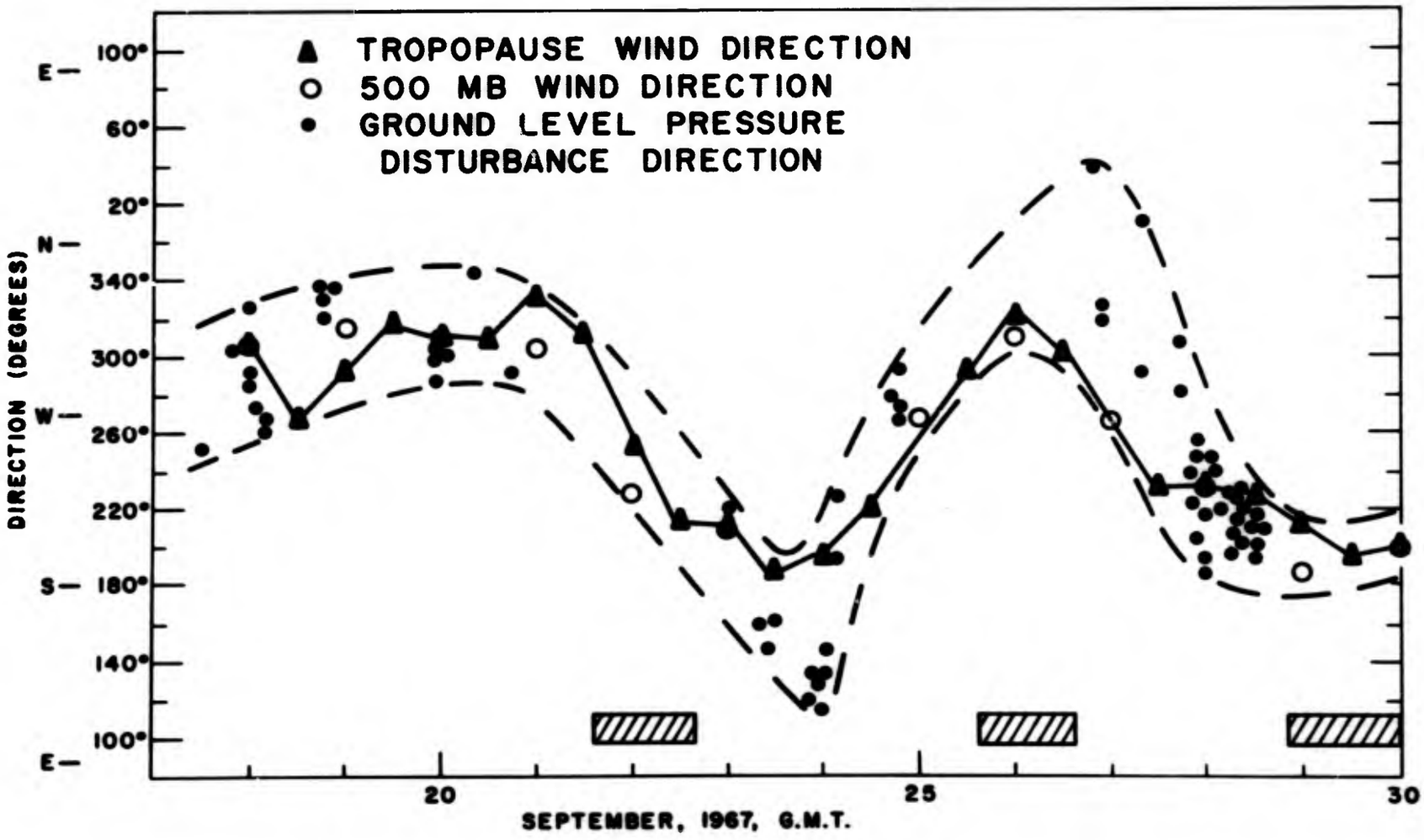

Fig. 15. Correlation of direction of movement of low-frequency pressure disturbances and direction of high-altitude tropospheric winds. Cross-hatched areas indicate sections of missing pressure data.

This level of coherence gave phase measurements which usually yielded low residuals in the least-squares fit. By further rejecting those least-square determinations whose residuals exceeded a specified value, it was possible to obtain plots such as shown in Fig. 15.

For this technique and for the array geometry of the inset of Fig. 1, speed determination is generally less accurate than direction determination; consequently, there is no detailed correlation of pressure disturbance speeds with jet-stream speeds (Fig. 16). However, from histograms showing the predominant speeds and periods of the disturbances (Fig. 17), it is seen that the speeds (10 to 50 m sec^{-1}) coincide with the usual tropopause wind speeds over Dobbs Ferry. Most of the moving disturbances had periods of about 32 to 96 min.

The observed speeds and periods of the jet-stream noise imply wavelengths of about 20 to 300 km with just over 100 km most common. Herron et al.[21] have shown, however, that the background noise decorrelates rapidly with distance. Spectral coherence values, for the periods of interest here, drop to a level of random coherence in 20 or 30 km, that is, in considerably less than one typical wavelength of the jet-stream noise. Such behavior indicates that the moving pressure disturbances are not <u>free</u> waves in the atmosphere.

There are, of course, sources of disturbance in the mesoscale range other than the jet stream, such as convective activity, free gravity waves, and, especially, disturbances associated with the passage of weather fronts. However, our observations indicate that jet-stream winds are the major source of continuous disturbance in our geographic area.

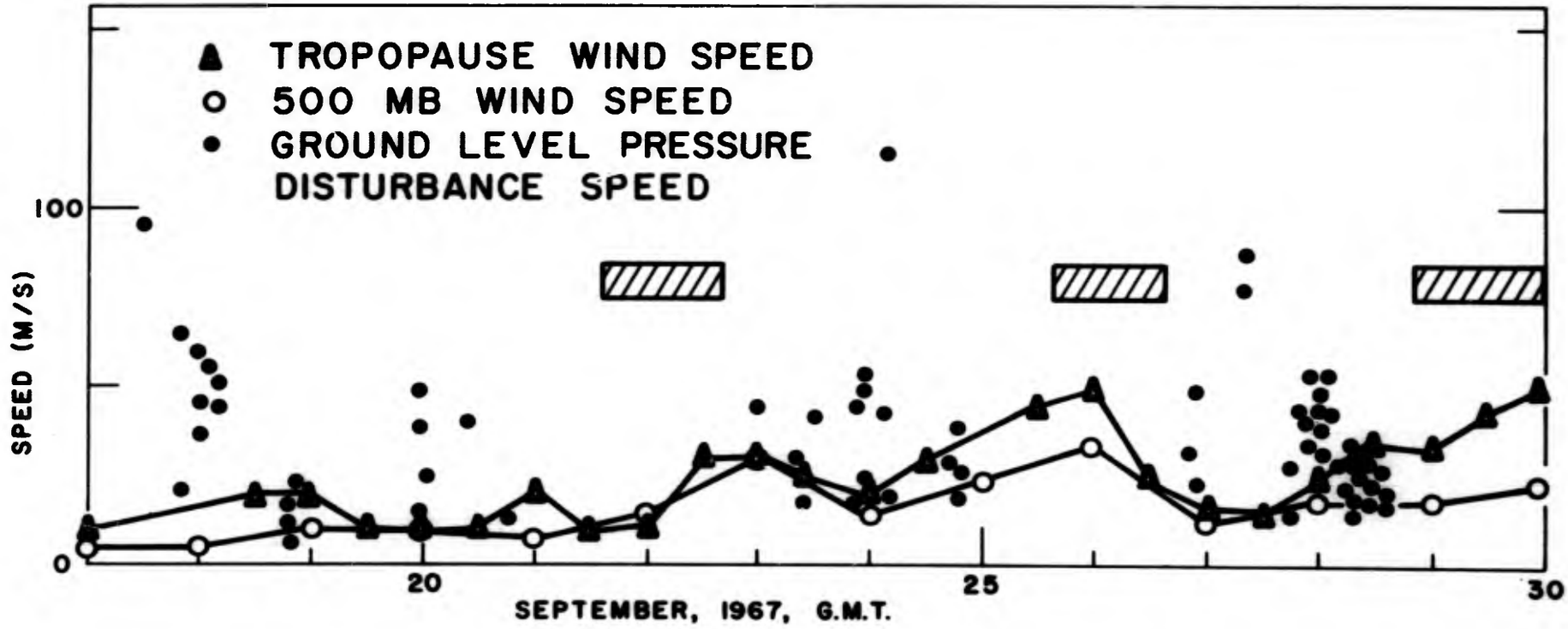

Fig. 16. Correlation of speed of low-frequency pressure disturbances and speed of high-altitude tropospheric winds.

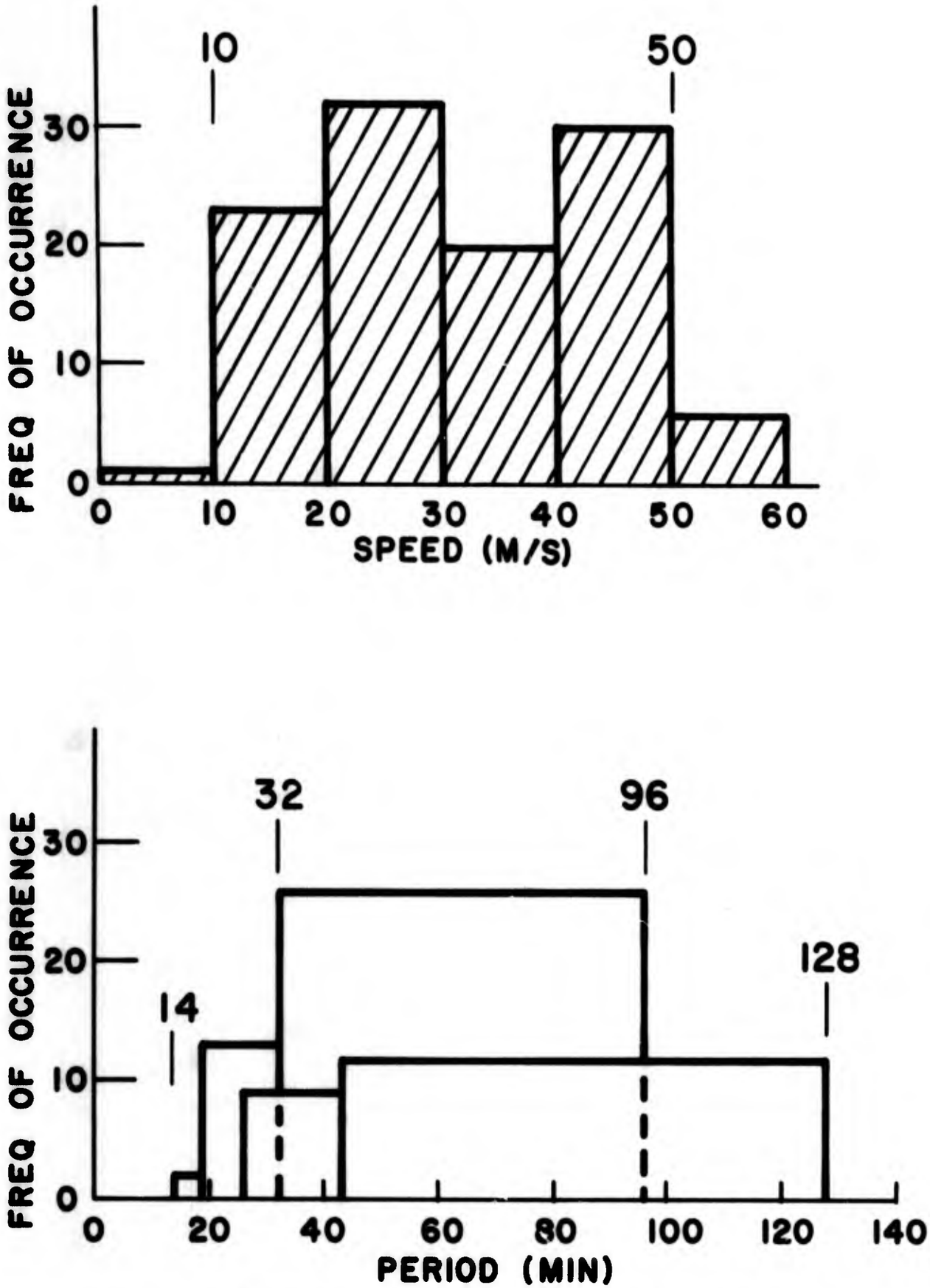

Fig. 17. Frequency of occurrences of the speeds and periods of background pressure fluctuations which correlate with jet-stream winds.

Experience in this study has indicated that the array of Fig. 1 is far from optimum. An array of several more stations, at slightly greater separations, with a geometry to take advantage of the prevailing direction of the jet stream might allow continuous tracking of the winds with considerable accuracy in direction and speed.

IV. CALCULATION OF GROUND-LEVEL PRESSURE SPECTRUM FROM JET-STREAM DATA

As pointed out above, a number of atmospheric pressure fluctuation power spectrums have been published and discussed in the literature during the last ten years.[2-5] The mechanisms supplying the energy depend upon the frequency band. Thus at periods of the order of days we have large-scale meteorological phenomena, and there are prominent peaks at the diurnal and semi-diurnal periods. At the short end, i.e., minutes and seconds, one is dealing both with background infrasonic activity and with boundary layer wind and turbulence effects. In between we have a range of periods from a few minutes to a few hours: this is the realm of mesoscale phenomena, some of the characteristics of which we have discussed above.

The energy input into this part of the spectrum is due to many causes and is quite variable. There is no single mechanism capable of accounting for all observed background pressure fluctuations. Nevertheless, it has long been a part of the folklore among students of infrasound that the tropospheric jet stream accounts for a good fraction of the observed pressure fluctuations at periods longer than a few minutes. Recent results confirm the intimate connection between jet-stream activity and mesoscale pressure fluctuations. It is quite common to see disturbances traveling with phase speeds of 10 to 50 m sec^{-1}, i.e., essentially with velocities of the order of jet-stream speeds, and whose directions of travel closely follow that of the jet-stream core aloft. This remarkable condition is often seen to persist for days or weeks. Thus there appears to be little doubt that, for long periods of time, most of the energy input into the mesoscale comes from the jet stream.

The purpose of this paper is to show that the energy input from the jet stream into ground-level pressure fluctuations may occur through a simple mechanism of internal gravity wave excitation by perturbations of the jet. Similar conclusions have been reached by others.[12-15] For example, Claerbout has suggested a relation between the velocity of the ground-level pressure disturbances and the wind speed at the height of minimum stability (i. e., lowest Richardson number) in the jet-stream cross sections; the best correlations may occur, according to him, with the velocity at a considerable distance upstream from the instrument. We have indicated above (section II) a possible correlation of spectrum levels with distance from the region of maximum eddy kinetic energy. We will now show that, using published jet-stream studies,[6, 7] and assuming some reasonable value for the velocity of the radiating disturbance (in the 10-50 m sec^{-1} range), the hypothesis of energy radiated into the internal gravity wave spectrum gives acceptable orders of magnitude for some of the observed properties of the mesoscale fluctuation fields.

Consider the wind velocity power spectrums obtained by aircraft measurements along the jet-stream axis.[6] We assume that these spectrums are stationary, and that they may be interpreted as a frozen-in property of the wind system carried along by the jet core. In order to calculate the spectral distribution of the ground-level pressure fluctuations due to the traveling jet-stream irregularities, we calculate first of all the effect of a simple traveling harmonic wave moving at jet-stream height with a phase velocity equal to some average jet-core wind speed. The atmosphere below this height is assumed to be stationary. Linear internal gravity wave theory then allows us to calculate the contribution of this spectral

component to the ground-level pressure power spectrum. Although this type of mechanism is admittedly unrealistic, it does give a surprisingly good estimate of the pressure fluctuation amplitudes. The ground-level period T is, of course, simply related to the wavelength λ and the assumed jet-core speed c by the usual equation

$$T = \lambda/c \quad . \tag{1}$$

Note that this method of connecting jet wind fluctuations to ground-level pressure spectrums does not assume a frozen-in perturbation field, only a frozen-in spectrum.

The pertinent elements of propagation theory are clear. We assume longitudinal horizontal and vertical wind fluctuation components u, w related by the condition of incompressibility. We assume a harmonic wave train, i.e., proportionality to $e^{i(\alpha x-\omega t)}$ where $\omega/\alpha = c$ is equal to the assumed jet-core velocity. The theory of internal gravity waves in a stratified fluid[22] tells us that, if

$$w \propto h\rho^{-1/2} \propto e^{i(\alpha x-\omega t)} \tag{2}$$

where ρ is the density, then, using the subscript z to denote differentiation

$$i\alpha u = -w_z \tag{3}$$

and

$$h_{zz} + \gamma^2 h = 0 \tag{4}$$

where

$$\gamma^2 = a^2\left(\frac{N^2}{\omega^2} - 1\right) - \frac{1}{4}\left(\frac{d}{dz}\ln\rho\right)^2 - \frac{1}{2}\frac{d^2}{dz^2}\ln\rho$$

$$\approx a^2\left(\frac{N^2}{\omega^2} - 1\right) = \frac{N^2}{c^2} - a^2 \quad . \tag{5}$$

Here N is the Väisälä frequency and c the phase velocity (equal to the assumed average jet-core speed). For order of magnitude calculations we assume that

$$N^2 = f(z) \tag{6}$$

with

$$N_1 \approx 1 \times 10^{-2} \text{ rad sec}^{-1} \text{ at ground level} \quad .$$

In order to calculate the pressure perturbation p at ground level due to a horizontal wind perturbation u_o in the jet stream we use, for the harmonic case

$$p = \rho c u \tag{7}$$

and the W. K. B. approximation:

$$h = \gamma^{-1/2} e^{\pm is}$$

$$s = \int_z^z \gamma \, dz \quad , \quad \gamma^2 > 0 \tag{8}$$

or

$$h = |\gamma|^{-1/2} e^{-s}$$

$$s = \int^z |\gamma| \, dz \quad , \quad \gamma^2 < 0 \tag{9}$$

with the result

$$u(z) = u_o \sqrt{\frac{\rho_o \gamma}{\rho \gamma_o}} \begin{pmatrix} \cos s & , & \gamma^2 > 0 \\ \text{or} & & \\ e^{-s} & , & \gamma^2 < 0 \end{pmatrix} \tag{10}$$

and

$$p(z) = c\sqrt{\rho \rho_o} \sqrt{\frac{\gamma}{\gamma_o}} u_o \begin{pmatrix} \cos s \\ \text{or} \\ e^{-s} \end{pmatrix} , \tag{11}$$

where the subscript o refers to values at jet-stream height. These results are only approximate, but should be quite adequate for order of magnitude calculations. A time average gives

$$\langle p^2 \rangle = c^2 \rho \rho_o \frac{\gamma}{\gamma_o} \begin{pmatrix} \cos^2 s \\ \text{or} \\ e^{-2s} \end{pmatrix} \langle u_o^2 \rangle . \tag{12}$$

Note the term in $\cos^2 s$, which predicts some <u>fine structure</u> for the spectrum, with <u>maxima</u> at points

$$s = n\pi . \tag{13}$$

In (10) - (12), we use the e^{-s} or $\cos s$ solutions depending upon whether the corresponding internal gravity waves are $(\gamma^2 < 0)$ or are not $(\gamma^2 > 0)$ totally reflected before reaching ground (Fig. 18). For example, corresponding to (a) in Fig. 18, assuming

$$N^2 = N_1^2 + az \tag{14}$$

we have, from (8) and (5):

$$s = \frac{2}{3} \frac{c^2}{a} \left(\gamma_o^3 - \gamma_1^3 \right) \tag{15}$$

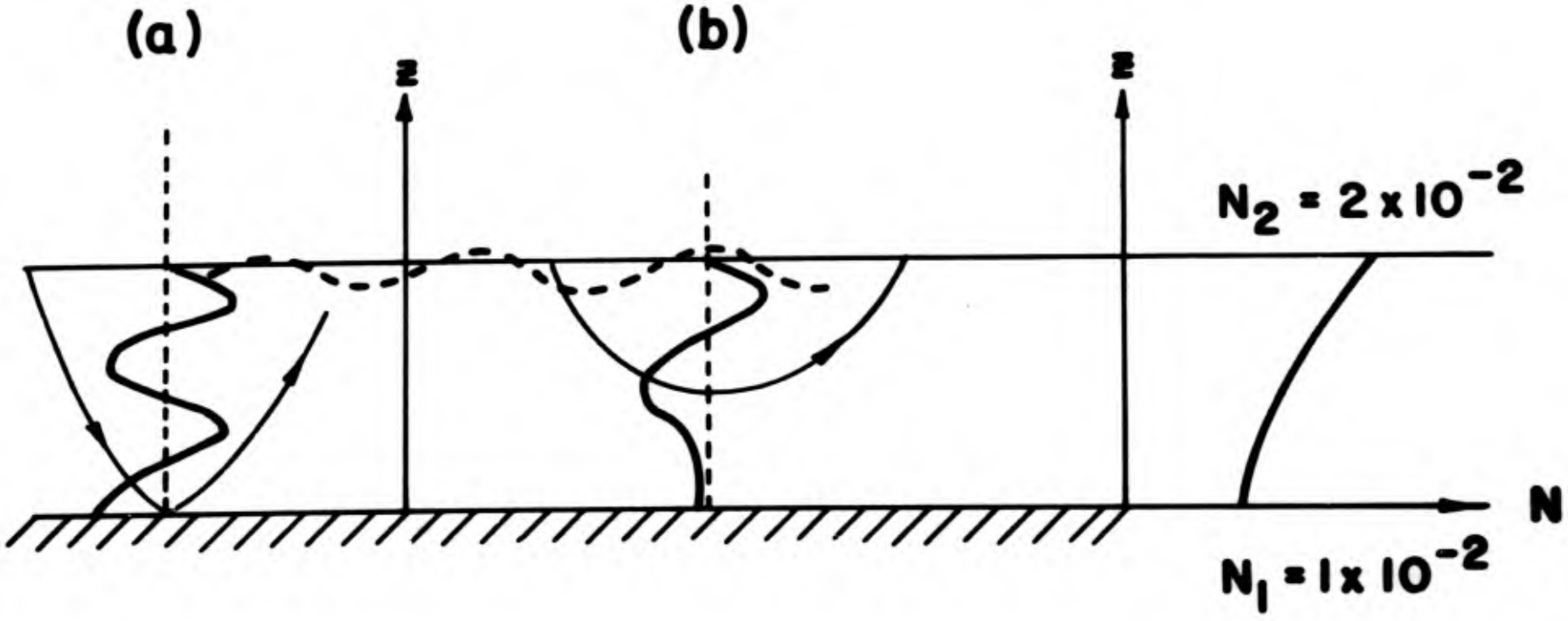

Fig. 18. Model with variable Väisälä frequency shown at night, may permit internal gravity waves to reach ground level (a) or may give total reflection at some intermediate level (b).

where γ_1 is the value of γ at ground level. On the other hand, for case (b) in Fig. 18, for which the wave energy is totally reflected at some height above Earth, we use e^{-2s} in (12) and

$$s = \frac{2}{3}\frac{c^2}{a}|\gamma_1|^3 \quad . \tag{16}$$

However, in calculated smoothed power spectrums (without fine structure) the $\cos^2 s$ terms in (10) - (12) are averaged and the result is not sensitive to the precise form of (14).

Assuming a density at $z = 10$ km of about 0.4 kg/m^3 and smoothing out the fine structure in (12) by taking $\overline{\cos^2 s} = 1/2$ gives (for $\gamma^2 > 0$) in MKSU

$$\Pi \simeq 0.2\, c^2 \frac{\gamma}{\gamma_o} P(u_o) \tag{17}$$

where Π is the power spectrum for the ground-level pressure perturbations and $P(u_o)$ is the wind velocity power spectrum in the jet stream. For the portion of the spectrum $\gamma^2 < 0$, i.e., $a > N/C$, corresponding to energy reflected before reaching ground we multiply (17) by e^{-2s}. In actual fact, the atmospheric density stratification is such that N is more nearly constant. The case of a static atmosphere with constant N corresponds to (17) with $\gamma = \gamma_o = \text{const}$, and calculations for $N = 1 \times 10^{-2}$ have been performed also.

We have applied this conversion to the power spectrum $P(u_o)$ given by Kao and Woods. Thus, their $E_{ss}(k)$ (Fig. 19) is related to $P(u_o)$ by

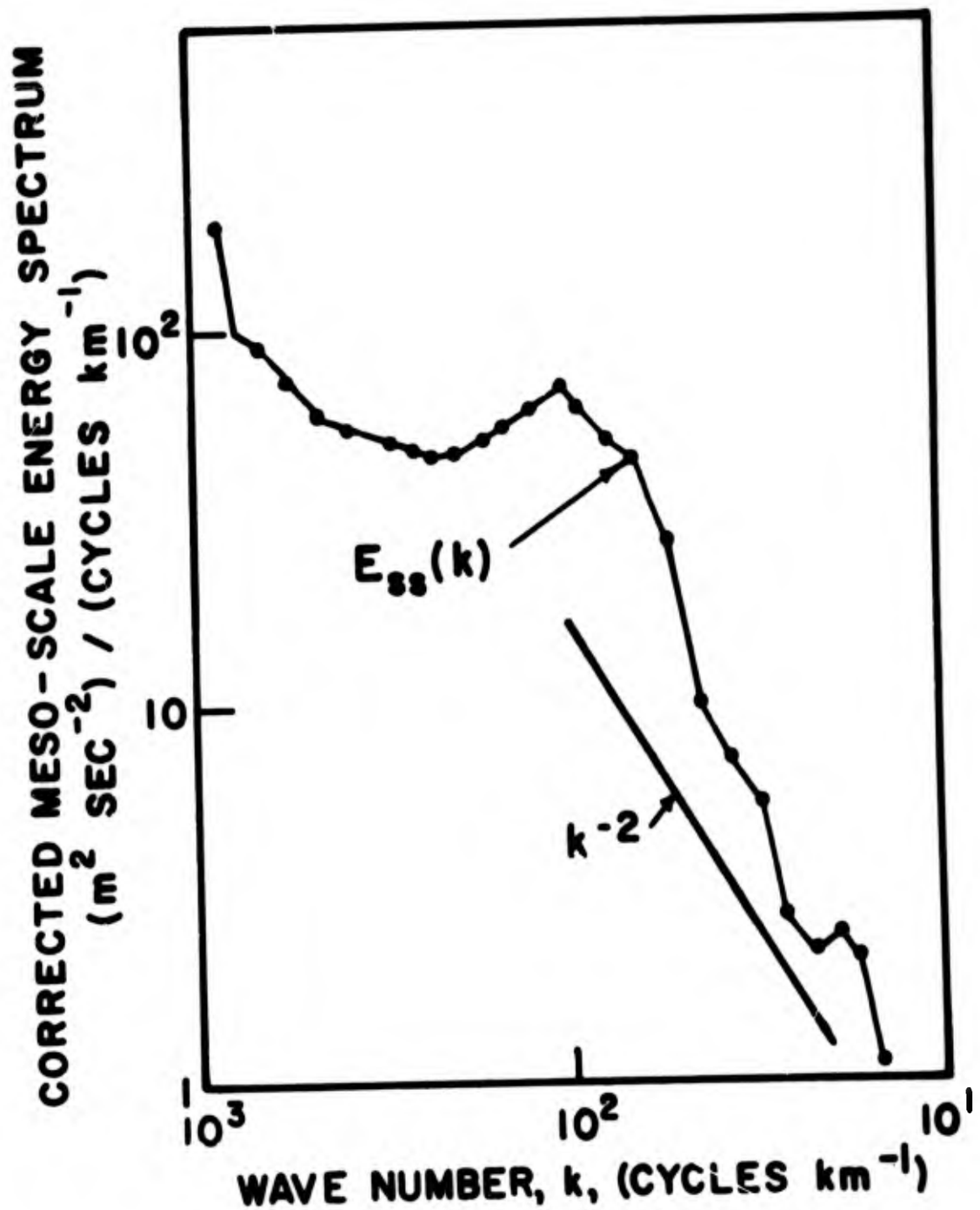

Fig. 19. The longitudinal power spectrum for longitudinal wind velocity fluctuations near the jet-stream core, as determined by Kao and Woods.[6]

$$P(u_o) = k E_{ss} \tag{18}$$

(where k is in cycles per km). Converting to $(\mu\text{bar})^2$ times cph and taking the log we obtain orders of magnitude comparable to those observed by us, as shown in Fig. 20. In this illustration the curves have been computed for two assumed jet-stream velocities of 20 and 40 m sec^{-1}. Dashed curves correspond to the model of Fig. 18 with $N_1 = 1 \times 10^{-2}$ rad sec^{-1} and $N(z) = 2 \times 10^{-2}$ at $z = 10$ km . The dotted curves correspond to a constant $N \simeq 1 \times 10^{-2}$.

The steep fall-off of the calculated spectrum for short periods corresponds in all cases to periods less than the ground-level Väisälä period. It is seen that the variable $N(z)$ model gives better results. This may well be due to the effects of wind shear, since classic hydrodynamic approximations[23] indicate that, for phase velocities higher than the local wind velocity U_o , we may sometimes replace the constant $\frac{N^2}{c^2}$ in (5) by $\frac{N^2}{c(c - U_o)}$.

Figure 20 shows that:

1. The assumption that ground-level pressure perturbations in the mesoscale region are primarily due to internal gravity waves excited by the jet-stream core provides a reasonable order of magnitude estimate of the observed fluctuation amplitudes.

2. This assumption is also in accord with the existence of observed changes in slope and humps in the power spectrum for the mesoscale range.

These very crude calculations are therefore at least consistent with observation. They also appear to explain the frequent appearance of fine-structure in the spectrum (see section III) since, by means of (13) it is

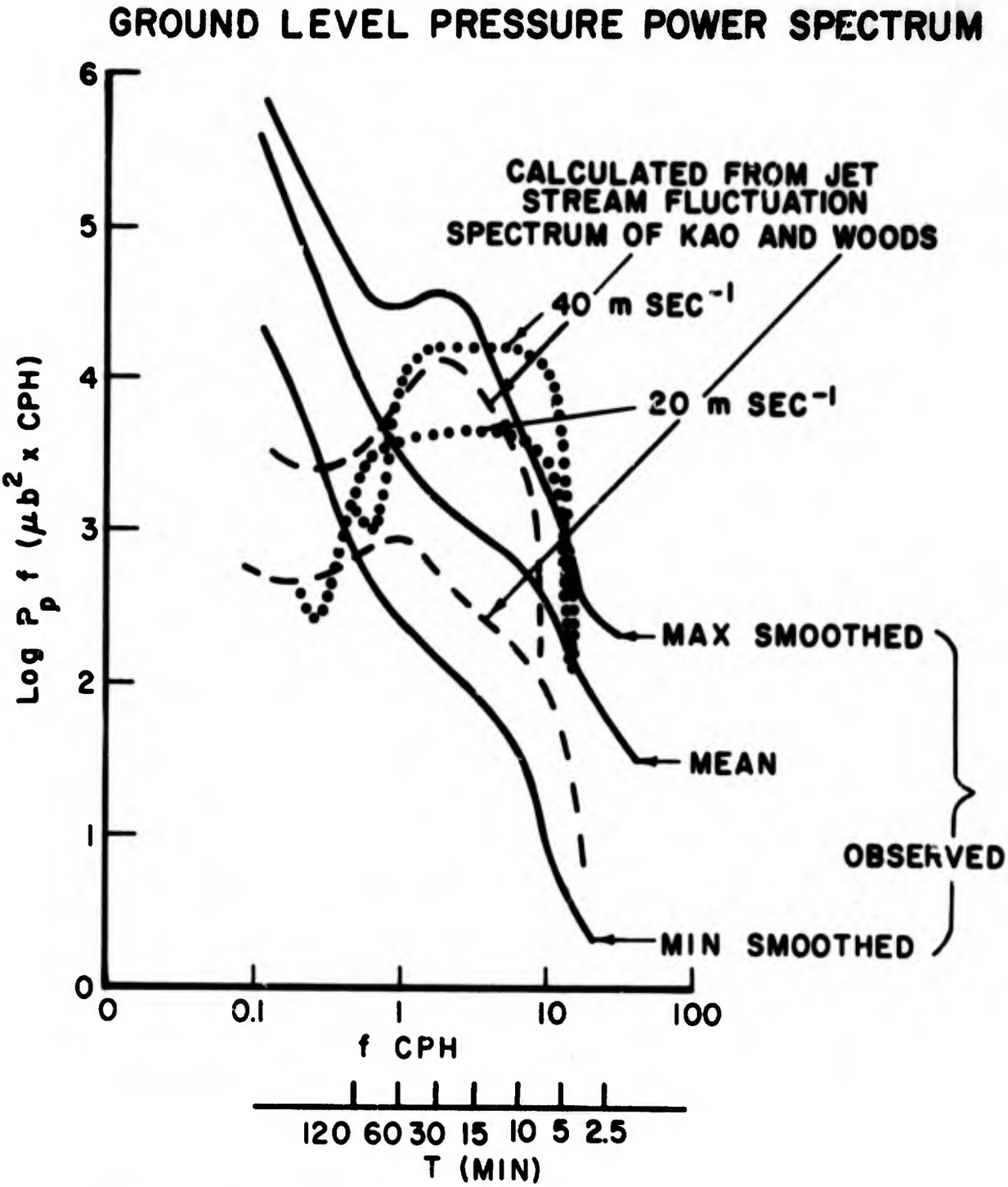

Fig. 20. Comparison of mean pressure power spectrums at ground level measured by Herron and Tolstoy with calculated spectrums for model of equation (6) (dashed lines) and for model with constant N (dotted line) obtained by applying the internal gravity wave radiation hypothesis to the Kao and Woods spectrum of Fig. 19. Maximum observed power spectrums are related to extreme weather conditions, and should not be representative of jet-stream activity.

easy to calculate the spacing and position of peaks in the spectrum. The results are sketched qualitatively in Fig. 21. The location and spacing of these spectral lines are consistent with many observations of unsmoothed spectrums (section III). A more quantitative elaboration of this point has not been attempted so far; in view of the numerous uncertainties and approximations besetting our model, detailed calculations of this kind would be premature.

This approach is also consistent with the peculiarly rapid decorrelation properties of the traveling disturbances observed in the Dobbs Ferry area: the mechanism proposed here implies that the correlation properties of pressure perturbations at ground level simply mirror the statistics of the jet-stream fluctuations. In other words, our pressure measurements at ground level are simply defining the correlation distances of the wind field in or near the jet-stream core.

Finally, wind-speed fluctuations produced at ground level by these internal gravity waves turn out to be very small: a simple calculation based upon (10) and the Kao and Woods spectrum gives a fluctuation level somewhat smaller than what one would deduce from published ground-level wind-speed spectrums.[17] Thus, here again, the hypothesis is in accord with existing data.

Note, however, that it is often possible to identify the appearance of slowly traveling wave trains having different origins, e.g., one observes similar disturbances originating near weather fronts, thunderstorms, and other violent perturbations of the atmosphere. It appears that these are frequently coherent over longer ranges than the typical jet-stream induced wave fields described above. Thus the calculations proposed here do not

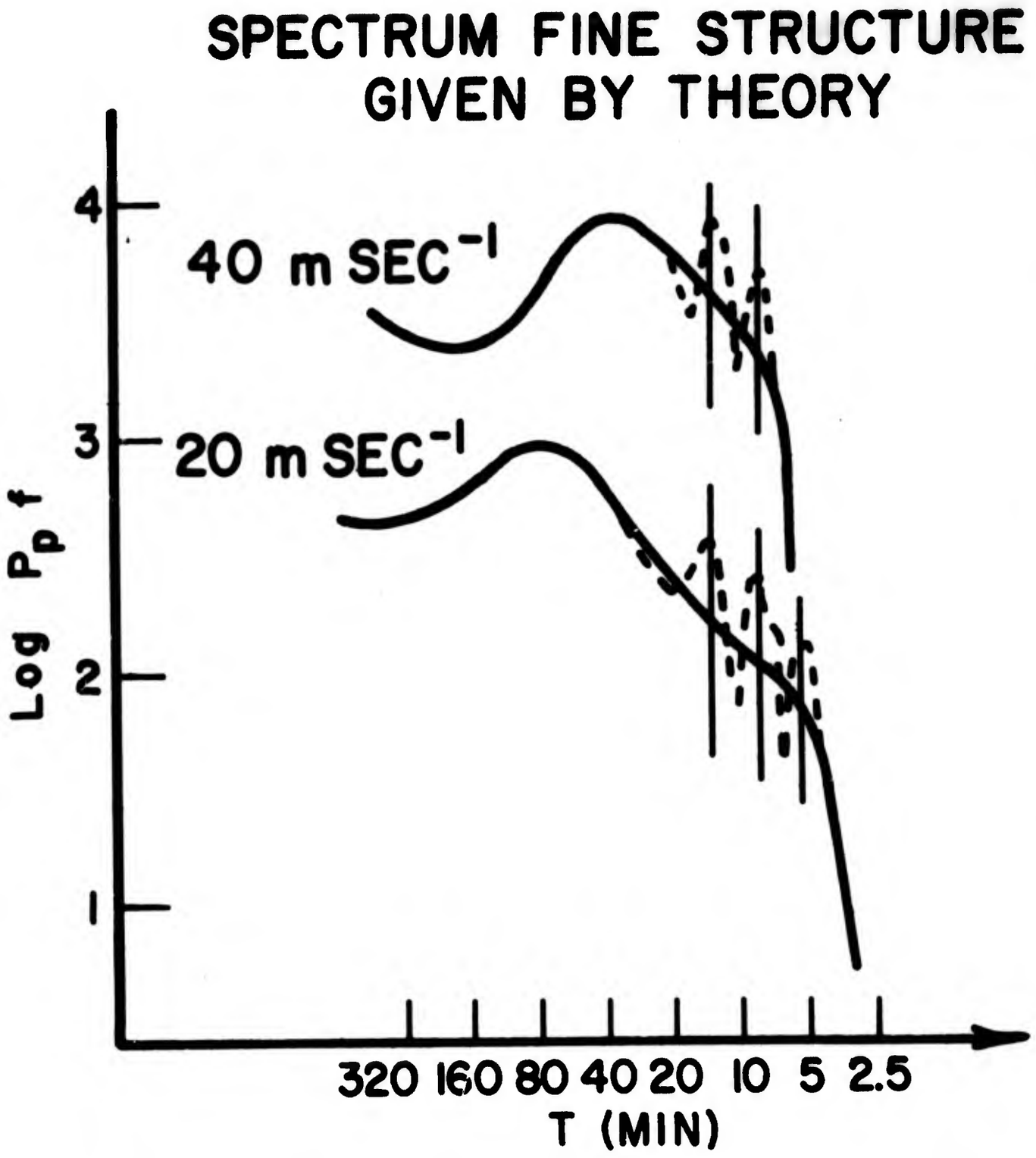

Fig. 21. Theoretical fine structure of power spectrum of ground level pressure perturbations.

purport to be relevant at all times, but only when no interference from severe meteorological conditions is likely. Our studies suggest that such conditions pertain more than 50% of the time in our area.

Finally, we should emphasize that it is actually surprising that the crude model we have used provides the correct orders of magnitude for ground-level pressure fluctuations. Certainly the image of each spectral component of the wind fluctuations in the jet stream acting as a traveling corrugation is highly questionable. The problem really is to explain why this model should work at all. Perhaps the wind fluctuations reported by Kao and Woods are due to an already fully developed field of internal gravity waves. In this case, our approximate model could be expected to yield the correct order of magnitude for the pressure fluctuations at ground level. The possibility remains also that stability waves in the shear flow below the jet stream may constitute a significant (but perhaps less efficient) mechanism for the transmission of these fluctuations.

V. A CLASS OF STABILITY WAVES

As a first stab at the whole problem of stability waves, we feel that the following discussion is pertinent.

We have seen that the effect of such waves may well be important in connection with jet-stream effects, and the theory described below represents an effort by one of us (E. Bendor) to shed some light on the problem. Note, however, that there exists another class of stability waves for those cases in which the second space derivative of the steady shear flow U_o'' does not vanish, corresponding to the sort of thing discussed extensively by Drazin and Howard,[24] and mentioned by one of us (I. Tolstoy[25]) in an article soon to appear in the Proceedings of the ESSA/ARPA 1968 Conference on Acoustic-Gravity Waves.

In the theory of hydrodynamic stability of parallel viscous flow it has been conventional to investigate the eigenvalues of the Orr-Sommerfeld problem for infinitesimal disturbances of real wave number, the criterion of stability being the sign of the imaginary part of the frequency. Gaster[26] and Watson[27] have pointed out that a procedure of more relevance to the usual experimental situation is to consider steady waves, which is to say, wave-like disturbances of real frequency but with spatially decaying (or growing) amplitudes. They referred to this as the "spatially dependent" problem, in contrast to the more familiar "time dependent" problem. For a given base flow the analysis in terms of normal modes is, of course, very similar in the two cases (the distinction arises mainly in the solution of the characteristic equation) and in fact the neutral stability boundary in the lowest mode is the same. Gaster[26] has

shown, by an argument based upon the orders of magnitude of certain growth factors found by Shen,[28] that for fixed Reynolds number, wavelength, and frequency the decay rates in the spatially and time dependent cases are related by the group velocity.

It has always been found (but has not been generally proved) that only the lowest eigenvalue of the Orr-Sommerfeld problem showed instability in a certain range of Reynolds number (R) and wave number (α) . It follows that if one is interested only in the question of stability then the cases of real α and real frequency ($\omega = \alpha\xi$) are equivalent, and the former is probably somewhat simpler since α enters the Orr-Sommerfeld equation and its solutions in a more complicated manner.

Another aspect of the subject arises, however, if one is interested not in stability but in actual wave propagation, in which case not only the decay (or growth) rates but also the dispersive properties are important. The present work was undertaken in the belief that this type of propagation in atmospheric shear layers might turn out to be just as significant as internal gravity waves, which have received far more attention (cf. Hines et al.[29]). In such an application the Orr-Sommerfeld problem must necessarily be cast in the form of steady waves and cannot be confined to the lowest mode; on the other hand, only the limit of large Reynolds number need be considered. To qualify physically as a phenomenon of wave propagation it must be shown that solutions exist, for $R \to \infty$, in which the damping ratio α_i/α_r (where $\alpha = \alpha_r + i\alpha_i$) is small at least for the lower eigenvalues. In the case of Couette flow, for example, this is already known to be the case, but the dispersion relations do not appear to have been investigated (cf. Grohne[30]). Although disturbances of small

positive damping have the more obvious physical significance, modes with slowly growing amplitude may also be said to constitute propagation provided, however, that no other disturbances are present which grow so rapidly as to destroy the base flow within a few wavelengths.

This type of atmospheric wave propagation has been the subject of research by a number of meteorologists; a summary of their work may be found in a book by Godske, Bergeron, Bjerknes, and Bungaard.[31] They coined the convenient name "stability waves" which appears also in this report. For the most part their work was on inviscid shear layers (although with consideration sometimes given to the effects of stratification, Coriolis forces, and compressibility), since it was believed that viscosity plays an important role only in the dissipation of such waves, but not in their formation and propagation. However, it is now known that in the viscous stability problem there are possible eigenvalues in the limit $R \to \infty$ in addition to those of the corresponding inviscid problem. The question of the proper formulation of the inviscid eigenvalue problem and its relation to the inviscid limit of the Orr-Sommerfeld problem is considerably beyond our scope here. It has been discussed by Case[32] and Lin[33] in some detail. (See also Case[34] specifically for Couette flow.) For the present we can do no better than to repeat a statement of Lin[8] also quoted by Case: "... there are certain damped solutions in a viscous fluid which, in the limit of vanishing viscosity, do not reduce to solutions of the inviscid equation throughout the whole region of flow." This is precisely what we shall find here in (C).* It also turns out that these damped solutions yield simple dispersion relations which are of considerable interest in the atmospheric application.

---

* See page 62.

Nevertheless, it cannot be claimed that the Orr-Sommerfeld problem constitutes a good physical model for atmospheric waves, since the important role of density stratification is not accounted for. If stratification and gravity as well as viscosity are included, the stability differential equation is still of the fourth order but is singular at the point where the flow and phase velocities are equal. If the effect of thermal conductivity is added, the singularity is removed but the equation is of the sixth order. In either case the mathematical difficulties become formidable. Koppel[35] has made some progress with the latter problem but was not able to carry it to the point of deriving a characteristic equation. Even this, of course, does not exhaust the possibly significant forces at work in the atmosphere. One could add Coriolis forces, for example. The solutions for such a general formulation would yield, in the appropriate limits of Richardson number, Prandtl number, etc., stability waves, internal gravity waves, Rossby waves, and so on.

In this report we shall consider only the simplest case, viz. the limit at large Reynolds number of waves in a layer of constant vorticity without stratification. (Waves in a stably stratified shear layer are likely on physical grounds to be more strongly damped than the present solutions indicate.) For such a shear layer the solutions to the Orr-Sommerfeld equation are well known and can be written down in the form of definite integrals. The spatially dependent Couette flow is considered first, followed by the problem of the shear layer between uniform streams.

Time dependent disturbances in Couette flow have been the subject of work by Grohne,[30] Hopf,[36] Wasow,[37] Deardorff,[38] and Gallagher and Mercer.[39] Although certain unresolved discrepancies exist at lower

Reynolds numbers between these various solutions, all indicate stability of plane Couette flow at all Reynolds numbers. The behavior of the eigenvalues is consistent with what we shall find here for spatially decaying waves; that is, the phase velocity ξ approaches the velocity of the bounding surface and the damping approaches zero as $R \to \infty$. The dispersion relation for steady waves in this limit is examined in (B).

The free shear layer, again in the time dependent case, has been investigated by Esch,[40] who arrived at a stability boundary in the α versus αR plane by a combination of analytical and numerical methods applied at large and small values of αR. He found unstable eigenvalues at all Reynolds numbers (down to zero) for sufficiently long waves. For $R \to \infty$ Esch's results reduce to

$$\alpha\xi = \pm \frac{1}{2} i \left[e^{-4\alpha} - (1 - 2\alpha)^2 \right]^{1/2} \tag{19}$$

which is the eigenvalue relation originally due to Rayleigh[41] for the inviscid shear layer, and he showed that the effect of viscosity is insignificant until αR falls below about 150. In the present work additional roots to the characteristic equation are found, the existence of which was only suspected by Esch, and which represent slightly damped "viscous" waves. Equation (19) indicates only that there is neutrally stable propagation when $\alpha > 0.64$, or, in dimensional terms, when the wavelength is less than about five shear layer thicknesses. It is of course to be expected on physical grounds that short wavelengths would be stable, but the low value of $\alpha = 0.64$ is convenient in the present context and lends the application to atmospheric propagation more plausibility than it would otherwise have had. Thus one could

postulate localized disturbances in which only higher frequencies are excited and for which the pattern of shear flow remains more or less intact for a large number of wavelengths.

For small α the velocity profile of the base flow cannot be important, since the shear layer then has the effect of a vortex sheet between uniform streams (cf. the Kelvin-Helmholtz instability in the inviscid case). In this connection one should mention the work of Drazin[42] on the stability of viscous flows with discontinuous velocity profiles in the presence of large wavelength disturbances. Drazin examined the validity of boundary conditions at discontinuities in the base flow velocity or velocity gradient of the type which were applied by Esch and are again applied here. He showed that it is justifiable to represent certain smooth profiles by discontinuous distributions if the wavenumber is small. In the present work, however, α is not necessarily small; in fact, the results are probably of most physical interest when $\alpha > 0.64$ for the lowest mode, as has already been pointed out. It is this consideration that prompted the investigation of the Couette flow case as a preliminary. The confluence of the solutions for that case and for the free shear layer which we shall find in the limit of large Reynolds number and mode number is one of the principal results of this chapter and appears to justify the representation of an atmospheric shear layer by a discontinuous velocity profile even when α is not small.

A. Solutions to the Orr-Sommerfeld Equation

We shall briefly set down the preliminaries to the Couette flow and free shear layer stability problems in a convenient form and then, in (B) and (C), go on to consider the eigenvalue relation in the limits which correspond to steady waves at large Reynolds number.

The base flow is $u_o^*(y) = Uy^*/L$ between infinite planes (or streams) at $y = \pm L$, moving in the x direction with velocity $\pm U$ respectively. All quantities are made dimensionless with respect to U and L, and $R = UL/\nu$ is the Reynolds number. Substitution of a stream function of the form $\phi(y) \exp i\alpha(x - \xi t)$ leads to the Orr-Sommerfeld equation

$$\phi'''' - 2\alpha^2\phi'' + \alpha^4\phi = i\alpha R(y - \xi)(\phi'' - \alpha^2\phi) \tag{20}$$

and for Couette flow the boundary conditions are

$$\phi(1) = \phi'(1) = \phi(-1) = \phi'(-1) = 0 \quad . \tag{21}$$

The boundary conditions for the free shear layer case are considered later.

It is clear from the symmetry of the base flow (or the invariance of (20) under simultaneous complex conjugation of α, ξ, and ϕ) that we need only consider waves traveling in the positive x direction. Let

$$\alpha = \alpha_r(1 + 3i\epsilon) \; ; \; \xi = \xi_r(1 - 3i\epsilon) \qquad \alpha_r > 0 \; ; \; \xi_r > 0 \tag{22}$$

so that 3ϵ is the "damping ratio" and disturbances are damped spatially if $\epsilon > 0$. (The factor 3 has been inserted here for later convenience and has no other significance.) The second of the equations in (22) follows from the first and the condition that the waves be steady ($\mathrm{Im}\,\alpha\xi = 0$). Note that we could equally well write $\alpha = \alpha_r \exp 3i\epsilon$, since we shall be concerned only with small damping. That this is consistent with the order of approximation of the results obtained can be confirmed later. We seek dispersion relations in the form $\alpha_r = \alpha_r(\epsilon, R)$, $\xi_r = \xi_r(\epsilon, R)$.

It will be most convenient for our purposes to express the solution of (20) in terms of integrals of Airy functions. The solution was first derived by Hopf,[36] who made use of the equivalent Hankel functions of order one-third. He obtained a complicated but essentially unrestricted characteristic relation between α, ξ, and R (for real α) and appears, in fact, to be the only author to have carried the problem to this point analytically. But according to Grohne[30] there are certain errors in Hopf's asymptotic representation of the solutions of (20), so that we cannot attempt to particularize his eigenvalue relation to the present problem. Instead we take the solution

$$\phi(y) = B_1 e^{\alpha y} + B_2 e^{-\alpha y} + B_3 \int_{-1}^{y} Ai(-z') \sinh\alpha(y - y') \, dy' + B_4 \int_{-1}^{y} Bi(-z') \sinh\alpha(y - y') \, dy' \tag{23}$$

where

$$z' = (\alpha R)^{-2/3} \{\alpha^2 + i\alpha R(y' - \xi)\} \tag{24}$$

and the B's are constants of integration. Ai and Bi are the Airy functions, with asymptotic expansions

$$Ai(-z) = -\frac{1}{2} i\pi^{-1/2} e^{i\pi/4} \left(s(z) + iz^{-1/2} s(z)^{-1}\right)\left(1 + 0(z^{-3/2})\right) \quad |z| \to \infty$$

$$Bi(-z) = \frac{1}{2} \pi^{-1/2} e^{i\pi/4} \left(s(z) - iz^{-1/2} s(z)^{-1}\right)\left(1 + 0(z^{-3/2})\right) \tag{25}$$

$$\text{in } -2\pi/3 < \arg z < 2\pi/3$$

where the notation

$$s(z) = z^{-1/4} \exp\left(\frac{2}{3} i z^{3/2}\right) \tag{26}$$

has been introduced. To carry out the integrations in equation (23) we have to consider the location in the z-plane of

$$\left.\begin{aligned} z_1 &= z(y=-1) = (a_r R)^{1/3} e^{i\epsilon}\left[\left(\frac{a_r}{R} - 3\epsilon\xi_r\right) - i\left(1 + \xi_r - \frac{3\epsilon a_r}{R}\right)\right] \\ z_2 &= z(y=1) = (a_r R)^{1/3} e^{i\epsilon}\left[\left(\frac{a_r}{R} - 3\epsilon\xi_r\right) + i\left(1 - \xi_r + \frac{3\epsilon a_r}{R}\right)\right] \end{aligned}\right\} . \tag{27}$$

In dealing with these integrations and the eigenvalue relations to be obtained in (B) and (C), we shall introduce approximations which must be valid if steady, slightly damped waves are to be found. Thus solutions of the characteristic equations for which a_r , ξ_r turn out to be other than pure real and positive in the limits $R \to \infty$, $\epsilon \to 0$ are inconsistent with these approximations and must be discarded. The remaining solutions (if any) represent stability waves if our approximations can be defended "a posteriori." Further, to obtain a physically meaningful result the function $a = a(\epsilon, R)$ must remain of $0(1)$ as $R \to \infty$, $\epsilon \to 0$. With this understanding, equation (27) indicates that if $a_r/3\xi_r R < \epsilon \ll (1 + \xi_r)/3\xi_r$ then

$$\arg z_1 = \frac{3\pi}{2} - \frac{\epsilon(2\xi_r - 1)}{1 + \xi_r} + O(R^{-1}) \quad . \tag{28}$$

The location of z_2 is less well defined; it will be in the second quadrant if $\epsilon(1 + 2\xi_r)/(1 - \xi_r) < \pi/2$. Nothing is known as yet about the order of z_2 . The path of integration passes to the left of the origin (which is a branch point of the asymptotic forms of the Airy functions) and

may be deformed into a contour lying in the left half of the z-plane on which $z \sim 0(R^{1/3})$ except possibly near z_2 . We require the asymptotic expansions of $Ai(-z)$, $Bi(-z)$ valid in $0 < \arg z < 4\pi/3$ and $2\pi/3 < \arg z < 2\pi$. These are easily obtained from (25) and the connection formulae for Airy functions, which may be found, for example, in Jeffreys and Jeffreys.[43] They are

$$Ai(-z) = \tfrac{1}{2}\pi^{-1/2} e^{i\pi/4} z^{-1/2} s(z)^{-1} \qquad |z| \to \infty \text{ in } 0<\arg z<4\pi/3 \text{ and } 2\pi/3<\arg z<2\pi$$

$$Bi(-z) = \tfrac{1}{2}\pi^{-1/2} e^{i\pi/4} \{2s(z) - iz^{-1/2} s(z)^{-1}\} \qquad |z| \to \infty \text{ in } 0<\arg z<4\pi/3$$

$$= \tfrac{1}{2}\pi^{-1/2} e^{i\pi/4} \{2s(z) + iz^{-1/2} s(z)^{-1}\} \qquad |z| \to \infty \text{ in } 2\pi/3<\arg z<2\pi \ .$$

Let

$$\mu = i a^{2/3} R^{-1/3}$$
$$Q = (aR)^{-1/3} \exp\{a(\xi + i a/R\} \quad ; \tag{29}$$

then the third and fourth solutions in (23) can be written

$$\begin{matrix} f_3 \\ f_4 \end{matrix} = \int_{-1}^{y} \begin{matrix} Ai(-z) \\ Bi(-z) \end{matrix} \sinh \mu(y - y') \, dy' = \frac{(aR)^{-2/3} e^{ay}}{2iQ} \int_{z_1}^{z} \begin{matrix} Ai(-z') \\ Bi(-z') \end{matrix} e^{\mu z'} \, dz'$$
$$- \frac{e^{-ay} Q}{2i} \int_{z_1}^{z} \begin{matrix} Ai(-z') \\ Bi(-z') \end{matrix} e^{-\mu z'} \, dz' \tag{30}$$

and their derivatives are

$$\begin{matrix} f_3' \\ f_4' \end{matrix} = \frac{a(aR)^{-2/3} e^{ay}}{2iQ} \int_{z_1}^{z} \begin{matrix} Ai(-z') \\ Bi(-z') \end{matrix} e^{\mu z'} \, dz' + \frac{a e^{-ay} Q}{2i} \int_{z_1}^{z} \begin{matrix} Ai(-z') \\ Bi(-z') \end{matrix} e^{-\mu z'} \, dz' \quad . \tag{31}$$

Some remarks should be made regarding these integrals. With the above asymptotic forms of $Ai(-z)$, $Bi(-z)$ they are of the form

$$\int z^{-1/4}\, e^{\pm\mu z} \exp\left(\pm\frac{2}{3}\, iz^{3/2}\right) dz \quad .$$

Successive integration by parts produces a doubly infinite series, convergent in powers of $\mu z^{-1/2}$, but asymptotic in powers of $z^{-3/2}$. Now Hopf,[36] who dealt with these same integrals, neglected $z^{-3/2}$ in relation to unity and therefore retained only the first convergent series in $\mu z^{-1/2}$. In the present case we must do the opposite; for if, as we shall show, $z_2 \sim 0(1)$ as $R \to \infty$, then $\mu z_2^{-1/2} \sim 0(R^{-1/3})$ and is negligible, whereas higher powers of $z_2^{-3/2}$ must be retained. The single asymptotic series obtained is related to the incomplete Gamma function, and the required integrals are

$$\int_{z_1}^{z_2} Ai(-z)\, e^{\pm\mu z}\, dz = \frac{1}{\sqrt{6\pi}} \left[e^{\pm\mu z_1}\, \Gamma\left(\frac{1}{2}; \frac{2iz_1^{3/2}}{3}\right) - e^{\pm\mu z_2}\, \Gamma\left(\frac{1}{2}; \frac{2iz_2^{3/2}}{3}\right) \right] \tag{32}$$

$$\int_{z_1}^{z_2} Bi(-z)\, e^{\pm\mu z}\, dz = \frac{i}{\sqrt{6\pi}} \left[e^{\pm\mu z_1} \left\{ 2\Gamma\left(\frac{1}{2}; -\frac{2iz_1^{3/2}}{3}\right) + \Gamma\left(\frac{1}{2}; \frac{2iz_1^{3/2}}{3}\right) \right\} \right.$$
$$\left. - e^{\pm\mu z_2} \left\{ 2\Gamma\left(\frac{1}{2}; -\frac{2iz_2^{3/2}}{3}\right) - \Gamma\left(\frac{1}{2}; \frac{2iz_2^{3/2}}{3}\right) \right\} \right] . \tag{33}$$

It should be noted that in writing incomplete Gamma functions here we refer specifically to their asymptotic expansions. The two solutions (32) and (33) will be required again in section (C) and have therefore been given here in somewhat more detail than is necessary for the Couette flow problem.

B. Couette Flow

For Couette flow (but not for the free shear layer) the boundary conditions at $y = -1$ require that $B_1 = B_2 = 0$. The eigenvalue relation is then simply

$$f_3(1)\, f_4'(1) = f_4(1)\, f_3'(1) \quad .$$

Now $\Gamma\left(\frac{1}{2}; -\frac{2iz_1^{3/2}}{3}\right)$ contains $s(z_1)$ as a factor and this is exponentially small if $5\pi/2 < \arg\left(iz_1^{3/2}\right) < 7\pi/2$, a sufficient condition for which, according to equation (28), is that $\pi/6 > (2\xi_r - 1)\,\epsilon/(1 + \xi_r) + 0(R^{-1})$. The remainder of the eigenvalue relation can be shown to reduce to

$$\sinh \mu(z_2 - z_1) \cdot \left[\Gamma\left(\frac{1}{2}; \frac{2iz_2^{3/2}}{3}\right) - \Gamma\left(\frac{1}{2}; -\frac{2iz_2^{3/2}}{3}\right)\right] = 0 \quad . \tag{34}$$

The first factor here gives $\alpha = k\pi i/2$; these are purely diffusive solutions which violate our assumptions and are in any case of no further interest in the present context. The required result is the expression in brackets. Suppose first that $|z_2| \gg 1$; then retaining only the leading two terms of the asymptotic series of the incomplete Gamma functions, we have

$$\exp\left(\frac{4}{3} iz_2^{3/2}\right) = -i\left\{1 - \frac{3}{2iz_2^{3/2}}\right\}$$

or

$$z_2 = \left(\frac{3\pi}{8}\right)^{2/3} (4k + 1)^{2/3}\, e^{2\pi i/3} \left\{1 - \frac{2z_2^{-3/2}}{\pi(4k + 1)}\right\} \qquad (k = 0, 1, 2 \ldots) \quad .$$

This last expression can be made definite by iteration, i.e.,

$$z_2 = \left(\frac{3\pi}{8}\right)^{2/3} (4k+1)^{2/3} e^{2\pi i/3}\left[1 + \frac{16}{3\pi^2(4k+1)^2}\right] \qquad (k = 0, 1, 2, \ldots) \quad . \quad (35)$$

Negative values of k place z_2 in a part of the z-plane inconsistent with our approximations and are therefore discarded.

The lowest approximation, derived in the above manner, gives $|z_2^{3/2}| = 3\pi/8$ for the lowest mode $(k = 0)$. For this value neither the iteration in (35) nor the representation of the integrals (32) and (33) by the asymptotic series of $\Gamma(\ )$ are sufficiently accurate. The asymptotic theory must be regarded as inadequate here, although one can probably derive a physically useful estimate of the properties of the lowest frequency mode of propagation. The second $(k = 1)$ and subsequent roots, however, are given with sufficient accuracy by (35) – certainly for present purposes. One could, of course, improve the estimate for the higher roots by retaining further terms in the series for the incomplete Gamma function, but this seems hardly worthwhile here. It should be mentioned at this point that even for $|z_2| = (3\pi/8)^{2/3}$ the second terms of the asymptotic series for $Ai(-z)$, $Bi(-z)$ are less than ten percent of the first terms, whereas in (35) the coefficient of $z_2^{-3/2}$ (for the first mode) is $2/\pi$. This will serve to explain why terms in $z_2^{-3/2}$ have been retained in (34), even though such terms have been discarded in (25) and (30).*

* These remarks apply essentially also to the free shear layer case and are therefore not repeated in (C).

On substituting (27) into (35) and extracting the modulus and argument we have

$$(\alpha_r R)^{1/3}\left[9\epsilon^2\xi_r^2 + (1-\xi_r)^2\right]^{1/2}\left\{1 + 0(\epsilon R)^{-1}\right\} = \left(\frac{3\pi}{8}\right)^{2/3}(4k+1)^{2/3}\left[1 + \frac{16}{3\pi^2(4k+1)^2}\right] \quad ; \quad \tan^{-1}\left(\frac{\xi_r - 1}{3\epsilon\,\xi_r}\right) + \epsilon + 0(\epsilon R)^{-1} = \frac{2\pi}{3} \quad .$$

These are the dispersion relations; they show that for small damping $(1 - \xi_r) \sim 0(\epsilon)$ and, since $\alpha_r \sim 0(1)$, $\epsilon \sim 0(R)^{-1/3}$. Grohne[30] obtained the analogous result in these limits for the time dependent Couette flow problem. The essentials of our result can be expressed by

$$\xi_r = 1 - 3\sqrt{3}\epsilon \quad ; \quad \alpha_r = \left(\frac{\pi}{16}\right)^2 \frac{(4k+1)^2}{6R\epsilon^3}\left[1 + \frac{16}{\pi^2(4k+1)^2}\right] \quad . \qquad (36)$$

C. The Free Shear Layer

We now attempt to find dispersion relations for waves in the parallel base flow

$$u_o = y \quad ; \quad |y| \leq 1 \ ,$$

$$u_o = \pm 1 \quad ; \quad y \geq 1 \ , \quad y \leq -1 \ , \text{ respectively.}$$

In the outer regions the equation

$$\phi'''' - 2\alpha^2\phi'' + \alpha^4\phi = i\alpha R(\pm 1 - \xi)(\phi'' - \alpha^2\phi)$$

has the solutions

$$\left.\begin{aligned} \phi &= A_1 e^{-ay} + A_2 e^{-b_2 y} \quad ; \quad y \geq 1 \\ \phi &= A_3 e^{ay} + A_4 e^{b_1 y} \quad ; \quad y \leq -1 \end{aligned}\right\} \tag{37}$$

where

$$\left.\begin{aligned} b_1 &= [a^2 - iaR(1+\xi)]^{1/2} \quad ; \quad \mathrm{Re}(b_1) > 0 \\ b_2 &= [a^2 + iaR(1-\xi)]^{1/2} \quad ; \quad \mathrm{Re}(b_2) > 0 \end{aligned}\right\} \tag{38}$$

and the remaining two pairs of solutions to this fourth order equation are discarded on applying the condition that $\phi \to 0$ as $|y| \to \infty$.

The solutions in $|y| \leq 1$ are given by equations (23) and (30). The nature of the boundary conditions to be applied at the discontinuities at $y = \pm 1$ is perhaps most clearly illustrated if we retrace the derivation to the step before the Orr-Sommerfeld equation. The small disturbance equations for the velocity and pressure fluctuations u, v and p in the base flow u_o are the continuity equation, $iau + v' = 0$, and the two momentum equations

$$R[-ia\xi u - iau_o u - vu_o'] = u'' - a^2 u - iaRp$$

$$R[-ia\xi v - iau_o v] = v'' - a^2 v - Dp' \quad .$$

Now, since u_o is continuous but u_o' discontinuous at $y = \pm 1$, it is possible to specify that solutions shall have discontinuities only in u'' , and therefore in ϕ'''' , with ϕ , ϕ' , and ϕ'' remaining continuous.

(For profiles with discontinuous u_o there must be a discontinuity in ϕ'' also.) That this leads to the proper formulation, at least for small α, has been shown by Drazin.[42] At $y = +1$ the first of the above two momentum equations then gives

$$Rv\left[(u_o')_{y=1+} - (u_o')_{y=1-}\right] = u''_{y=1+} - u''_{y=1-}$$

with a similar relation at $y = -1$. Hence

$$i\alpha R\phi_{y=1} = \phi'''_{y=1+} - \phi_{y=1-}$$

$$-i\alpha R\phi_{y=-1} = \phi'''_{y=-1+} - \phi_{y=-1-}$$

where $\phi_{y=1-}$ and $\phi_{y=-1+}$ signify the solutions in $|y| \leq 1$. These conditions, together with the solutions (37) and the requirement that ϕ, ϕ', ϕ'' remain continuous at $y = \pm 1$, lead to the following boundary conditions:

$$\left.\begin{aligned}
&\phi''(1) + (b_2 + \alpha)\,\phi'(1) + b_2\alpha\phi(1) = 0\\
&\phi'''(1) - \left(b_2^2 + \alpha b_2 + \alpha^2\right)\phi'(1) + \left(i\alpha R - b_2^2\alpha - \alpha^2 b_2\right)\phi(1) = 0\\
&\phi''(-1) - (b_1 + \alpha)\,\phi'(-1) + b_1\alpha\phi(-1) = 0\\
&\phi'''(-1) - \left(b_1^2 + \alpha b_1 + \alpha^2\right)\phi(-1) + \left(i\alpha R + b_1^2\alpha + \alpha^2 b_1\right)\phi(-1) = 0
\end{aligned}\right\} \quad . \quad (39)$$

These are the four boundary conditions which together with the solutions in (23) constitute the eigenvalue problem for the free shear layer. Esch[40] obtained these four relations by considering the limits of integrals of the full Orr-Sommerfeld equation across the region separating the shear

layer from the uniform streams. In terms of f_3 and f_4 and their derivatives the characteristic determinant here is of course the same as that given by Esch. But to obtain f_3 and f_4 he applied the method of steepest descent to the inverse Fourier transforms of these functions. Such a procedure would appear to be less convenient in the present context than the Airy function approach, which facilitates the evaluation of the orders of magnitude of the various terms in the characteristic determinant in the limit of large Reynolds number. In any case, f_3, f_4, f'_3, and f'_4 are already given by equations (30) through (33), and

$$f''_3 = a^2 f_3 + 2a\,Ai(-z) \quad ; \quad f'''_3 = a^2 f'_3 - 2ai(aR)^{1/3} dAi(-z)/d(-z)$$

$$f''_4 = a^2 f_4 + 2a\,Bi(-z) \quad ; \quad f'''_4 = a^2 f'_4 - 2ai(aR)^{1/3} dBi(-z)/d(-z)$$

where primes still denote differentiation with respect to y. To obtain the asymptotic expansions of the derivatives of the Airy functions it need only be noted that $dAi(-z)/d(-z) \to iz^{1/2} Ai(-z)$ as $|z| \to \infty$ except near the positive real axis, and that the Wronskian $W[Ai(-z), Bi(-z)] = \pi^{-1}$. The characteristic determinant then follows on substituting equations (30) through (33) and these last few relations into (39). Before writing the determinant down two further points should be noted. First, to simplify the notation somewhat, that

$$Q\, e^{+a}\, e^{-\mu z_1} = Q\, e^{-a}\, e^{-\mu z_2} = (aR)^{-1/3}$$

and

$$-b_1 = (aR)^{1/3} z_1^{1/2} \quad ; \quad b_2 = (aR)^{1/3} z_2^{1/2}$$

where the signs preceding b_1, b_2 have been chosen so as to make $\mathrm{Re}(b_1) > 0$, $\mathrm{Re}(b_2) > 0$. Secondly, we expect, as in the case of Couette flow, that $\epsilon(2\xi_r - 1)/(1 - \xi_r) < \pi/6$, in which case s_1 and $\Gamma\left(\frac{1}{2}; -\frac{2iz_1^{3/2}}{3}\right)$ are again exponentially small. Then, neglecting terms with these factors, the determinant is

$$\begin{vmatrix} b_2+a & 0 & -i\lambda(b_2+a)\left(e^{2a}\Gamma_1^+ - \Gamma_2^+\right) & \lambda(b_2+a)\left(e^{2a}\Gamma_1^+ + \Gamma_2^+ - 2\Gamma_2^-\right) \\ & & +z_2^{-1/2}s_2^{-1} & +2s_2 - iz_2^{-1/2}s_2^{-1} \\ i\frac{R}{2} & i\frac{R}{2}e^{-2a} & \frac{1}{2}\lambda R(e^{2a} - e^{-2a})\Gamma_1^+ & \frac{1}{2}i\lambda R(e^{2a} - e^{-2a})\Gamma_1^+ \\ & & +2(aR)^{1/3}s_2^{-1} & -2i(aR)^{1/3}s_2^{-1} \\ 0 & b_1+a & z_1^{-1/2}s_1^{-1} & iz_1^{-1/2}s_1^{-1} \\ i\frac{R}{2}e^{-2a} & i\frac{R}{2} + b_1(b_1+a) & (aR)^{1/3}s_1^{-1} & i(aR)^{1/3}s_1^{-1} \end{vmatrix} = 0 \qquad (40)$$

where the notation

$$\lambda = \sqrt{2/3}\, e^{-i\pi/4}(aR)^{-1/3}$$

$$\Gamma_{1,2}^{\pm} = \Gamma\left(\frac{1}{2}; \pm\frac{2iz_{1,2}^{3/2}}{3}\right)$$

has been introduced.

The next step, obviously, is to multiply the third column of (40) by i and to subtract it from the fourth column. Some caution is necessary

here, since we are dealing with the difference between exponentially large terms (i.e., s_1^{-1} and Γ_1^+), which are themselves only asymptotic approximations. This step can be justified, however, by going back to the original Airy functions and their integrals and making use of the fact that

$$\mathrm{Bi}(-z) - i\mathrm{Ai}(-z) = -\frac{1}{2} i e^{i\pi/3} \mathrm{Ai}(-ze^{-2\pi i/3}) \tag{}$$

which is exponentially small as $R \to \infty$ for $\arg(z_1)$ as given by equation (28).

Now consider the four elements in column three of (40). Each element contains a term in s_1^{-1} or Γ_1^+ (of which s_1^{-1} is a factor). Two of the elements also contain terms in s_2^{-1} (or Γ_2^+, of which s_2^{-1} is a factor), which may also be exponentially large as $R \to \infty$, since $\arg(z_2)$ is not yet known. To show that these terms may be neglected we write

$$\left|\frac{s_1}{s_2}\right| = \left|\frac{z_2 \Gamma_2^+ g\left(-2iz_1^{3/2}/3\right)}{z_1 \Gamma_1^+ g\left(-2iz_2^{3/2}/3\right)}\right| \tag{41}$$

$$= \left|\frac{z_2^{1/4}}{z_1^{1/4}}\right| \exp\left[\frac{2}{3}\left|z_1^{3/2}\right| \cos\arg\left(iz_1^{3/2}\right)\left\{1 - \left|\frac{z_2^{3/2}}{z_1^{3/2}}\right| \frac{\cos\arg\left(iz_2^{3/2}\right)}{\cos\arg\left(iz_1^{3/2}\right)}\right\}\right]$$

where $g(\ )$ is the asymptotic series with leading term unity arising in the incomplete Gamma function, viz.,

$$g(p) = 1 + \frac{1}{2} p^{-1} + \frac{1.3}{2^2} p^{-2} + \frac{1.35}{2^3} p^{-3} + \ldots \quad . \tag{42}$$

It is easily shown from equation (27) that $|z_2/z_1| < 1$ for $1 < \xi_r < 3\epsilon a_r R^{-1}$, and that

$$\cos \arg\left(iz_2^{3/2}\right) / \cos \arg\left(iz_1^{3/2}\right) < 1$$

if $\epsilon \sim 0(R^{-k})$ as $R \to \infty$ with $k < 1$. The expression (41) is then exponentially small when s_1 is exponentially small, so that s_1^{-1} may be cancelled from (40), which becomes, finally:

$$\left[\lambda b_2 \left(1 + \frac{a}{b_2}\right)\left(\Gamma_2^+ - \Gamma_2^-\right) + s_2 - iz_2^{-1/2} s_2^{-1}\right]\left[b_1^2\left(1 + \frac{a}{b_1}\right) + i\frac{R}{2}\left(1 + \frac{a}{2b_1}\right)\left(1 - e^{-4a}\right)\right]$$

$$+ 4(aR)^{1/3} R^{-1} s_2^{-1} b_2 \left(1 + \frac{a}{b_1}\right)\left(1 + \frac{a}{b_2}\right)\left(b_1^2 + i\frac{R}{2}\right) = 0 \quad . \tag{43}$$

We shall now see what eigenvalues may be extracted from this characteristic equation.

The "Inviscid" Eigenvalue

Suppose first that ξ does not approach unity as R increases. Then $z_2 \sim 0(R^{1/3})$ and $b_2 \sim 0(R^{1/2})$ as $R \to \infty$. The functions $\Gamma_2^{\pm}$ are therefore given correct to $0(R^{-1/2})$ by their first terms only. In this case no transcendental functions remain in (43), which may be written

$$0 = h_o(a, \xi) + (aR)^{-1/2} h_1(a, \xi) + (aR)^{-1} h_2(a, \xi) + \text{etc.} \quad , \tag{44}$$

with

$$h_o(a, \xi) = 4a^2\xi^2 + e^{-4a} - (1 - 2a)^2 \quad .$$

Thus in the inviscid limit we have recovered the result

$$h_o(a,\xi) = 0$$

which is just the inviscid solution of Rayleigh, i. e., equation (19). Esch[40] calculated the roots of the first three terms of (44) but found that the contributions of $h_1(a,\xi)$ and $h_2(a,\xi)$ were insignificant for aR greater than about 150. It should be pointed out that the correct form of the functions h_1, h_2 cannot be derived from equation (43), since these should contain contributions from higher order terms of the asymptotic expansions of the original Airy functions. But we are not here interested in anything beyond the inviscid limit of the above characteristic relation.

The "Viscous" Eigenvalues

Next suppose that $(1 - \xi) \sim 0(R^{-1/3})$ as $R \to \infty$. Then $z_2 \sim 0(1)$, $b_2 \sim 0(R^{1/3})$, and further terms in the series of $\Gamma_2^{\pm}$ must be retained. If one now considers the orders of magnitude of the terms in equation (43) it appears that

$$\left[\lambda b_2\left(\Gamma_2^+ - \Gamma_2^-\right) + s_2 - iz_2^{-1/2} s_2^{-1}\right]\left[\frac{b_1^2}{R} + \frac{i}{2}\left(1 - e^{-4a}\right)\right] = 0(R^{-1/3}) \quad .$$

The second factor here cannot yield a solution for which $z_2 \sim 0(1)$. We require the roots of the first factor, which is to say, the roots of

$$\exp\left(\frac{4}{3} iz_2^{3/2}\right) = i \frac{1 + g\left(-2iz_2^{3/2}/3\right)}{1 - g\left(2iz_2^{3/2}/3\right)} \quad . \tag{45}$$

There will be one root in every interval 2π of $\mathrm{Im}\left(4iz_2^{3/2}/3\right)$; but only the semi-infinite set for which $\mathrm{Im}\left(4iz_2^{3/2}/3\right) < 0$ can lead to damped

solutions $(\epsilon > 0)$ in which $\xi_r \lesssim 1$. No significance can be attached to the remaining set in the present theory.

Here again the asymptotic theory is not really adequate for the calculation of the first root, for which the series $g\left(\pm 2iz_2^{3/2}/3\right)$ start to diverge already after the third term. For the second and subsequent roots it is sufficiently accurate for our purposes (in the atmospheric application) to truncate (45) to

$$\exp\left(4iz_2^{3/2}/3\right) = 8z_2^{3/2}/3 \quad . \tag{46}$$

In spite of its simplicity there appears to be no tabulation of the roots of this equation. We have therefore computed the first sixteen roots of (46), which are presented in the following table. The phase velocity and wavenumber, in the present approximation, are given by equation (27) and the values in the table. They are

$$\xi_r = 1 + 3\epsilon \tan(\arg z_2)$$

$$a_r = -\frac{|z_2|^3 \cos^3(\arg z_2)}{27 R \epsilon^3}$$

and the group velocity is

$$\frac{\partial(a\xi)}{\partial a} = 1 - 2\epsilon\left(i - \tan(\arg z_2)\right) \quad .$$

The asymptotic behavior of the roots for large mode number k is of particular interest here, since we wish to compare small wavelength propagation with the Couette flow results. If we write

$$z_2^{3/2} = \frac{3}{2}\pi k(1 + \gamma\kappa)\, e^{i(\pi+\beta_\kappa)}$$

where k is a positive integer, then it is easily shown that

$$\beta_\kappa \sim \ln(4\pi k)/2\pi k \quad ; \quad \gamma_\kappa \sim \frac{1}{2k}\left(1 + \beta_\kappa^2\right)$$

for large k . Thus for the higher modes we have

$$\left.\begin{aligned} \xi_r &= 1 - 3\sqrt{3}\,\epsilon + 8\beta_\kappa\epsilon \\ \alpha_r &= \left(\frac{\pi}{16}\right)^2 \frac{1}{6R\epsilon^3}(4k + 2)^2(1 + 2\sqrt{3}\,\beta_\kappa) \end{aligned}\right\} \tag{47}$$

and this is just the Couette flow result as $k \to \infty$. Finally, neglecting β_κ , equations (47) can be combined to express the dispersion relation in the more conventional form

$$\alpha = \omega + \frac{(9\pi^2)^{1/3}}{4}(4k + 2)^{2/3} e^{i\pi/6} R^{-1/3} \omega^{2/3} \tag{48}$$

where ω is the (real) frequency.

TABLE

Roots of $\exp\left(4iz_2^{3/2}/3\right) - 8z_2^{3/2}/3 = 0$

k	$\lvert z_2 \rvert$	$\arg z_2/\pi$
0	1.758	0.533
1	3.423	0.600
2	5.213	0.620
3	6.510	0.630
4	7.688	0.636
5	8.781	0.640
6	9.810	0.644

TABLE (continued)

k	$\lvert z_2 \rvert$	$\arg z_2/\pi$
7	10.788	0.646
8	11.724	0.648
9	12.624	0.650
10	13.492	0.651
11	14.334	0.652
12	15.152	0.653
13	15.948	0.654
14	16.725	0.654
15	17.484	0.655

D. Discussion

We have shown that slightly damped steady waves propagate in a high Reynolds number shear flow at a phase velocity approaching the maximum velocity in the layer and have given the dispersion relations. Perhaps the most interesting feature of these waves is that for higher modes their dispersive properties cease to be influenced by the boundary, i. e., they were found to be the same for the free shear layer as for Couette flow. This result is of course entirely to be expected. From a mathematical point of view it is an instance of the asymptotic behavior of eigenvalues and eigenfunctions. Physically, we have an example of the distinction between "intrinsic" dispersion and "geometric" dispersion, which arises frequently in other branches of fluid mechanics (e. g., sound waves in layered media) or physics. The latter is due to the mutual interference of waves reflected from the boundaries, whereas the former does not depend on the presence of boundaries at all and is due to the anisotropies of the medium - in this case the velocity gradient of the base flow. As the wavelength decreases in relation to the width of the layer so the contribution of "geometric" dispersion becomes weaker.

These remarks naturally lead one to ask what happens if there is one solid boundary (at $y = -1$, say) and one uniform stream (in $y \geq 1$). The eigenvalue relation then follows from the third and fourth solutions in (23) and the first two of the boundary conditions (39). On passing to the limit $R \to \infty$ and assuming again that $z_2 \sim 0(1)$, it turns out that one obtains precisely the same result as in the free shear layer case, i.e., equation (45). Actually, for both these two cases, it can be shown that the problem reduces to that of finding the roots z_2 of the equation

$$Bi(-z_2) - iAi(-z_2) - iz_2^{1/2} e^{-\mu z_2} \int_{\infty e^{3\pi i/2}}^{z_2} [Bi(-z) - iAi(-z)]\, e^{\mu z} dz = 0(R^{-1/3}) .$$

This, however, is not evident at first; the asymptotic theory is required to examine the orders of magnitude of the various terms in the characteristic determinant. Thus one could, if desired, dispense with the asymptotic method thereafter and compute the roots of the above equation directly and hence derive dispersion relations in the limit $R \to \infty$ to any desired degree of accuracy.

In accordance with the remark of Lin[8] previously quoted, we have found two distinct sets of solutions for the free shear layer. The first yield, in the inviscid limit, the secular equation of Rayleigh, previously recovered by Esch.[40] The second set is always viscous in character, is always stable, and represents stability waves of the type which are of interest in the atmospheric application. Why Esch was unable to obtain that branch of his "time-dependent" secular equation which corresponds to our equation (45) is not clear. He appears to have been quite aware of the probable existence of other solutions and noted that he searched for

them both analytically and numerically. His presentation is somewhat terse, so that it has not been possible to discover where in his work these solutions vanished.

It is of some interest, in discussing propagation in the atmosphere, to consider how the above results might be extended to account for the presence of a vorticity gradient. There must again be a discrete spectrum of eigenvalues associated with solutions which remain viscous in character even in the limit of large Reynolds number. If the base flow $u_o(y)$ is continuously differentiable these solutions must be regular throughout the domain of flow, since they satisfy the full Orr-Sommerfeld equation. Then, if $u_o(y)$ has a Taylor expansion

$$u_o(y) = u_o(y_o) + u_o'(y_o)y + \frac{1}{2}u_o''(y_o)y^2 +$$

about some point $y = y_o$ the characteristic equation can be written

$$F(\alpha, \xi, R, u_o(y_o), u_o'(y_o), u_o''(y_o), \ldots) = 0$$

and must be regular in $u_o(y_o), u_o'(y_o)$, etc. Hence for fixed α and R the roots ξ of the characteristic equation $F(\alpha, \xi, R, u_o(y_o), u_o'(y_o))$ for a parallel flow with constant vorticity must be the limits, as $u_o''(y_o), u_o'''(y_o)$, etc., tend to zero, of the eigenvalues of the more general flow. Evidently the physically significant quantities are the ratios $u_o''(y_o)/\alpha$, etc., and as these vanish the dispersive properties of waves in any smoothly varying velocity distribution must approach those found here for the free shear layer. These remarks obviously do not apply to those solutions which in the limit $R \to \infty$ satisfy the corresponding inviscid Rayleigh equation.

Although the waves found here for the free shear layer can only be slightly damped, it has not, of course, been proved that unstable solutions do not exist. It is unlikely that there exist solutions for which $\xi_r \to 1, \epsilon \to 0$ as $R \to \infty$, with $\epsilon < 0$ (which, as has already been pointed out, could also represent "propagation"). To investigate this point it would be necessary to repeat the whole derivation of (C) with different asymptotic representations of the Airy functions. If this is done for Couette flow (where it is already known that there are no such solutions) one finds that $\xi_r \sim 0(\epsilon^{-1})$ as $R \to \infty$, which is in conflict with the well-known theorem that the phase velocity cannot be greater than the maximum flow velocity. It is likely that a similar inconsistency would arise in the case of the free shear layer. On physical grounds such a result is also improbable, since it would imply instability at all wavenumbers consistent with the approximations, whereas it is always found that disturbances are stable for sufficiently small wavelengths. If these conjectures are correct the steady waves of (C) are the only long wavelength stability waves which can propagate at a phase velocity $\xi_r \approx 1$. For short wavelengths there is also the Rayleigh secular equation (19), which becomes $\xi = 1 - 1/2\alpha$ and therefore represents undamped waves with similar phase velocity but different dispersive properties.

Finally, we should briefly examine the order of magnitude of events in the context of an atmospheric shear layer. The Reynolds number is typically 10^7 to 10^9. Leaving aside the lowest mode, which is unreliable, we find that for $\epsilon = 0.01$ the phase velocities of the next two modes are 0.907U and 0.924U and the amplitude falls to e^{-1} of its initial value in five wavelengths. This is already a rather high degree of damping. With

$R = 10^7$ the wavelengths of these two modes are 1140L and 242L, which for typical values of L might be comparable to the wavelengths of long-period internal gravity waves (cf. Hines et al.[29]). For $R = 10^9$, $\epsilon = 0.001$ we get $\xi_r = 0.990, 0.992$ and wavelengths of 114L and 24L respectively for the same two modes. In this case the amplitude is attenuated by a factor e^{-1} in about fifty wavelengths. These values illustrate, incidentally, the strong dependence of damping on the departure of the phase velocity from the velocity of the bounding uniform streams. This effect is obviously connected with the fact that as $\xi_r \to 1$ the wave motion penetrating the region $y > 1$ reduces, in a frame moving with the velocity of that region, to a stationary displacement of the fluid particles.

VI. CONCLUSIONS

We may conclude from the above discussions that:

1. A good fraction of the pressure fluctuation background in the 2-90 min period passband is generated by the jet stream or, more generally, by the tropospheric wind system at the 300-200 mbar levels. That this is so has been fairly common knowledge among workers in the field since the 1950's. Our own studies, described in sections II and III, provide some new and detailed quantitative data on this subject. Of considerable interest is the fact that the direction of motion of pressure perturbations across a small array follows very closely that of the jet-stream core aloft.

2. It also appears probable that most of this jet-stream-generated activity corresponds to an internal gravity wave field radiated by the wind system fluctuations. This point of view is upheld by some simple calculations converting jet-stream wind fluctuation spectrums to a ground-level pressure spectrum (section IV).

3. The preceding hypothesis helps also in explaining the often observed and curiously rapid decorrelation of pressure perturbations in this passband over microbarograph arrays of modest dimensions. Decorrelation over distances appreciably less than a wavelength is quite common in the Dobbs Ferry area. This is due to the fact that the gravity wave field simply maps the wind fluctuation system at jet height into a ground-level pressure system so that the pressure perturbation statistics mirror, in some sense, the jet-stream perturbation statistics.

4. The jet-stream wind system viewed in cross-section is approximately a steady shear flow with a sharp peak near the 10-12 km level above

ground, and it is clear that the effects of the shear flow must be important in determining the properties of the pressure field radiated by the jet stream. As pointed out in section IV of this report, there is some indication of this in the fact that, in our static internal gravity wave model for the pressure field, it is found that a Väisälä frequency $N(z)$ increasing with height gives the best results, whereas a constant N would be more consistent with measured temperature distributions in standard atmospheric models. However, this is only a first cut at the problem.

A detailed study of the effects of stability waves in shear flows is highly desirable at this point. Section V represents one line of attack on this kind of problem: the Orr-Sommerfeld equation for the case of plane Couette flow enables one to obtain preliminary dispersion laws for the case where viscosity plays a dominant role.

Another possible approach to these problems will be sketched in a forthcoming paper in the Proceedings of the ESSA/ARPA Symposium.[25] It is shown there that stability waves of a different class can exist in the inviscid case when the second derivative of the steady flow does not vanish. Further theoretical efforts along these lines should be actively encouraged since not only do naturally occurring shear flows sustain propagating pressure disturbances, but also the behavior of gravity and acoustic waves in the presence of strong shears is not sufficiently understood.

5. From both experimental and theoretical points of view, a great deal remains to be done to achieve an understanding of traveling low-frequency pressure perturbations. The large scale array of microbarographs shown in Fig. 1 is especially well suited to the study of 5-20 min periods in the 200-600 m sec^{-1} range. The average spacing of the sensors is such that

the jet-stream activity should be essentially uncorrelated, and beamforming techniques are very useful for studying other sources of waves. Tentative results indicate the existence of long wavelength systems (10^2-10^3 km) having velocities in the 100-600 m sec^{-1} range. A very thorough study of these is planned for FY 1969.

6. Finally, some detailed studies of the background in the 2-0.1 min period passband would be highly desirable to fill the gap which now exists between our studies and the traditional boundary-layer turbulence studies of the micrometeorologist.

VII. REFERENCES

1. C. S. Clay and D. W. Kraft, Microbarographs for the Measurement of Atmospheric Waves, (Hudson Laboratories Tech. Rept. No. 135, 1967).
2. J. L. Lumley and H. A. Panofsky, The Structure of Atmospheric Turbulence (Interscience Publishers, New York, 1964), 239 p.
3. E. E. Gossard, "Spectra of atmospheric scalars," J. Geophys. Res. 65, 3339-3351 (1960).
4. G. S. Golitsyn, "On the time spectrum of micropulsations in atmospheric pressure," Izv. Geophys. Ser. 8, 1253-1258 (1964).
5. N. Z. Pinus, E. R. Reiter, G. N. Shur, and N. K. Vinnichenko, "Power spectra of turbulence in the free atmosphere," Tellus, 19(2), 206 (1967).
6. S. K. Kao and H. D. Woods, "Energy spectra of mesoscale turbulence along and across the jet stream," J. Atmos. Sci. 21, 513 (1964).
7. E. Reiter, Jet-Stream Meteorology (Univ. of Chicago Press, 1963), 515 p.
8. C. C. Lin, The Theory of Hydrodynamic Stability (Cambridge Univ. Press, 1955), 155 p.
9. W. L. Donn, P. L. Milic, and R. Brilliant, "Gravity waves and the tropical sea breeze," J. Meteorol. 13, 356-361 (1956).
10. R. H. Clarke, "Pressure oscillations and fallout downdraughts," Quart. J. Roy. Meteorol. Soc. 88, 459-469 (1962).
11. A. D. Pierce and S. C. Coroniti, "A mechanism for the generation of acoustic-gravity waves during thunderstorm formation," Nature 210, 1209-1210 (1966).

12. J. M. Young, "Experimental observations of tropospheric jet stream waves" (A), Proc. ESSA/ARPA Acoustic-Gravity Wave Symposium, Boulder Colorado (1968).

13. J. F. Claerbout, Electromagnetic Effects of Atmospheric Gravity Waves (Massachusetts Institute of Technology thesis, 1967).

14. T. R. Madden and Jon Claerbout, "Observations of jet stream gravity waves and their implications concerning jet stream stability" (A), Proc. ESSA/ARPA Acoustic-Gravity Wave Symposium, Boulder, Colorado (1968).

15. R. K. Cook, "Subsonic atmospheric oscillations" (A), Proc. ESSA/ ARPA Acoustic-Gravity Wave Symposium, Boulder, Colorado (1968).

16. R. B. Blackman and J. W. Tukey, The Measurement of Power Spectra (Dover Pub., 1958).

17. I. Van der Hoven, "Power spectrum of horizontal wind speed in the frequency range from 0.0007 to 900 cycles per hour," J. Meteorol. 14, 160-164 (1957).

18. T. J. Herron and I. Tolstoy, "Tracking jet stream winds from ground-level pressure signals," to appear in J. Atmos. Sci. (1968).

19. S. K. Kao and W. P. Hurley, "Variations of the kinetic energy of large-scale eddy currents in relation to the jet stream," J. Geophys. Res. 67, 4233-4242 (1962).

20. S. K. Kao and G. R. Farr, "Turbulent kinetic energy in relation to jet streams, cyclone tracks, and ocean currents," J. Geophys. Res. 71, 4289-4296 (1966).

21. T. J. Herron, I. Tolstoy, and D. W. Kraft, "Atmospheric pressure background fluctuations in the mesoscale range," to appear in J. Geophys. Res. (1968).

22. I. Tolstoy, "The theory of waves in stratified fluids, including the effects of gravity and rotation," Revs. Mod. Phys. 35, 207-230 (1963).

23. C. S. Yih, Dynamics of Nonhomogeneous Fluids (Macmillan Co., New York, 1965).

24. P. G. Drazin and L. N. Howard, "Hydrodynamic stability of parallel flow of inviscid fluid," in Advances in Appl. Mech. 9 (Academic Press, New York, 1966).

25. I. Tolstoy, "Mesoscale pressure fluctuations in the atmosphere," Proc. ESSA/ARPA Acoustic-Gravity Wave Symposium, Boulder Colorado (1968).

26. M. Gaster, J. Fluid Mech. 14, 222-224 (1962).

27. J. Watson, J. Fluid Mech. 14, 211-221 (1962).

28. S. F. Shen, J. Aero. Sci. 21, 62 (1954).

29. C. O. Hines, I. Paghis, T. R. Hartz, and J. A. Fejer, Physics of the Earth's Upper Atmosphere (Prentice Hall, Inc., 1965).

30. D. Grohne, Z. angew. Math. Mech. 34, 344-357 (translated as N.A.C.A. Tech. Memo. 1417) (1954).

31. C. L. Godske, T. Bergeron, J. Bjerknes, and R. C. Bungaard, Dynamic Meteorology and Weather Forecasting (The Waverly Press, Inc., 1957).

32. K. M. Case, J. Fluid Mech. 10, 420-429 (1961).

33. C. C. Lin, J. Fluid Mech. 10, 430-438 (1961).

34. K. M. Case, Phys. Fluids 3, 143-148 (1960).

35. D. Koppel, J. Math. Phys. 5, 963-982 (1964).

36. L. Hopf, Annalen der Physik 44, 1-60 (1914).

37. W. Wasow, J. Res. Nat. Bur. Standards 51, 195-202 (1953).

38. J. W. Deardorff, J. Fluid Mech. 15, 623-631 (1963).

39. A. P. Gallagher and A. McD. Mercer, J. Fluid Mech. 18, 350-352 (1964).

40. R. E. Esch, J. Fluid Mech. 3, 289-303 (1957).

41. Lord Rayleigh, Theory of Sound (Dover Pub., 1945).

42. P. G. Drazin, J. Fluid Mech. 10, 571-583 (1961).

43. Sir H. Jeffreys and B. S. Jeffreys, Methods of Theoretical Physics (Cambridge Univ. Press, Cambridge, 1956).

UNCLASSIFIED

Security Classification

DOCUMENT CONTROL DATA - R & D

(Security classification of title, body of abstract and indexing annotation must be entered when the overall report is classified)

1. ORIGINATING ACTIVITY (Corporate author) Hudson Laboratories of Columbia University 145 Palisade Street Dobbs Ferry, New York 10522	2a. REPORT SECURITY CLASSIFICATION UNCLASSIFIED 2b. GROUP Not applicable

3. REPORT TITLE

SUMMARY REPORT, ATMOSPHERIC PROPAGATION BACKGROUND STUDIES UP TO SEPTEMBER 1, 1968

4. DESCRIPTIVE NOTES (Type of report and inclusive dates)

Technical Report

5. AUTHOR(S) (First name, middle initial, last name)

Ivan Tolstoy, T. Herron, E. Bendor, and D. W. Kraft

6. REPORT DATE	7a. TOTAL NO. OF PAGES	7b. NO. OF REFS
September 1968	88	43

8a. CONTRACT OR GRANT NO.	9a. ORIGINATOR'S REPORT NUMBER(S)
Nonr-266(84) b. PROJECT NO.	Technical Report No. 158
c. d.	9b. OTHER REPORT NO(S) (Any other numbers that may be assigned this report)

10. DISTRIBUTION STATEMENT

Document cleared for public release and sale; its distribution is unlimited.

11. SUPPLEMENTARY NOTES	12. SPONSORING MILITARY ACTIVITY
	Office of Naval Research, Code 466 Advanced Research Projects Agency

13. ABSTRACT

After a brief description of the system, a summary is given of significant results obtained in describing properties of background pressure fluctuations in the Dobbs Ferry area. Particular emphasis has been given, during the last year or so, to understanding the effect of the tropospheric jet stream. It is shown, among other things, that a good part of this effect is probably due to the generation of internal gravity waves by the wind structure near the 300 mbar level. This mechansim is sensitive to wind shears. Finally, although the exact importance of stability waves in this picture is hard to ascertain as of now, a preliminary investigation of one class of stability waves is reported.

14 KEY WORDS	LINK A		LINK B		LINK C	
	ROLE	WT	ROLE	WT	ROLE	WT
internal gravity waves microbarograph arrays atmospheric pressure background noise atmospheric waves jet-stream pressure fluctuations atmospheric stability waves						